Technical University of Crete

School of Mineral Resources Engineering

Postgraduate Program in Petroleum Engineering

Msc Thesis:

Modeling Single & Multi-phase flows in petroleum reservoirs using Comsol Multiphysics: ''Pore to field-scale effects''

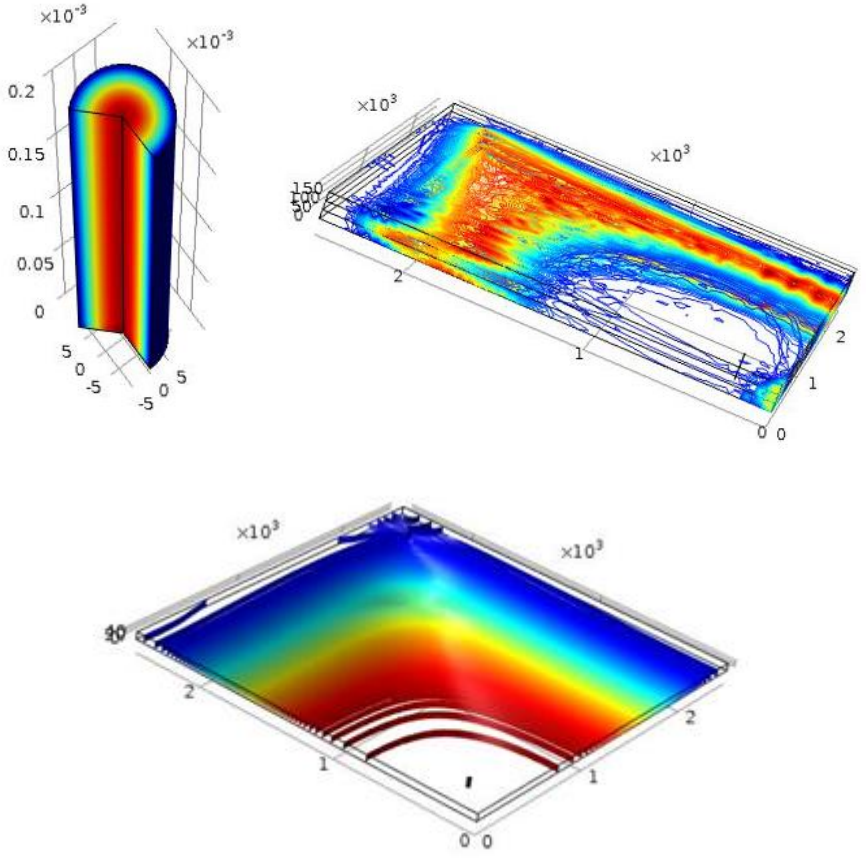

Pandis Konstantinos Dionysios

Chemical Engineer

September 2015

Chania

Advisors: Dr. Ch.Chatzichristos, Dr. A. Yiotis

Table of contents

List of figures

List of tables

Acknowledgements

I place on record, my sincere thank you to Dr. Ch.Chatzichristos and Dr. A. Yiotis, for their support and encouragement.

I would like to thank the School of mineral resources of the faculty of engineering of Crete for the opportunity to conduct my Msc thesis on the National Center of Scientific Research "DEMOKRITOS".

I would also like to thank my family and Eirini for their support and patience.

Abstract

The numerical modeling of transport processes in stratified petroleum reservoirs is a task of significant importance in the oil production industry as it is involved in technologies related to both reservoir characterization and recovery optimization. Traditional modeling

approaches rely on the treatment of the porous material of the reservoir as an effective continuum, where fluxes are related to the gradients of volumed-average scalar properties, such as pressure, concentration, phase saturation and temperature, through macroscopic (cores scale) parameters, such as the medium permeability (or relative permeabilities for multi-phase flows), effective diffusivities etc. Such approaches essentially ignore the accurate description of pore scale phenomena arising at the complicated geometry of the pore scale in favor of reduced computational time for such field scale problems.

Modeling of transport processes at the pore scale is however an indispensable tool for the calculation of macroscopic transport parameters, as an alternative to core and field scale experimental measurements. The objective of this Msc thesis, is thus to offer better physical insight on how pore scale effects such as hydrodynamic dispersion determine the field scale transport properties in such upscaled systems. This will be accomplished using a commercially available generic finite element solver numerical modeling tool; Comsol Multiphysics. The results will be then implemented at realistic reservoir scale systems to study two processes relevant to reservoir characterization and recovery optimization; non-Gaussian hydrodynamic dispersion and water-flooding.

Pore-scale modeling is a first step to study single and multiphase flows and transport in porous media. The hydrodynamic dispersion coefficient is calculated for a single capillary, in order to simulate the phenomenon emanating at the pore scale. Mass transfer in the field scale and therefore in three dimensions is simulated in the second model, in order to extract information about dispersion in three dimensions and about the effects arising in a stratified, anisotropic and heterogeneous geometry, such as those typically encountered in petroleum reservoirs. As a last step, two phase flow is simulated in a three dimensional reservoir focusing primarily on the displacement of the non-wetting (oil) from the wetting phase (water) in the course of a Waterflooding process, used to optimize oil recovery in pressure depleted reservoirs.

The above numerical simulations are performed using a commercially-available software; Comsol Multiphysics. The Comsol multiphysics software utilizes PDEs to model the above physical phenomena. The system of equations, which are implemented in the software, consists of mass balances, partial differential equations that describe the accumulation, transport, injection and production of the phases in the model. In addition, several auxiliary equations apply to the system, coupling the different phases in the system together. This set of equations, PDEs and auxiliary equations, allows for equation manipulation such that the main differences between the formulations are the dependent variables that are solved for.

A comparison with the results of Eclipse simulator, which is widely used in the oil recovery industry, will be also provided in the case of two phase flow in a petroleum reservoir. Finally the aim is to evaluate the possibility of whether Comsol Multiphysics can reproduce the results provided by commercial reservoir simulators such as Eclipse 100.

Chapter 1: An introduction to transport processes in Petroleum Reservoirs

1. Petroleum Reservoir

A petroleum reservoir or oil and gas reservoir is a subsurface quantity of hydrocarbons contained in porous or fractured rock formations. The naturally occurring hydrocarbons, such as crude oil or natural gas, are trapped in the subsurface by overlying rock formations with lower permeability (caprocks). The total estimate of petroleum reservoirs includes the total quantity of oil that be can be recovered and oil residuals that cannot be recovered, due to geographical constraints and reservoir/oil characteristics and financial/technological limitations. The fraction of crude oil reservoirs that can be extracted from the oil field using current technology is classified as reserves. In order to maximize the oil recovery from a field, various techniques are used during the lifetime of a reservoir.

2. Oil Recovery technologies

Oil recovery technologies can be divided into three different types, which are explained below. Water injection is a secondary recovery method.

Primary recovery is the natural depletion of the reservoir (Green and Willhite, 1998).This means that oil is recovered with the help of the natural energy present in the reservoir, namely the pressure build-up during its formation process. Examples are solution-gas drive, gas-cap drive, natural water drive, fluid and rock expansion and gravity drainage. This form of production is used at the beginning of a reservoirs production period. Primary recovery is the least expensive method of extraction and typical recovery factors during this process is 5-15% of original oil in place (OOIP).

Secondary recovery is the augmentation of natural energy with the injection of water or gas (Green and Willhite, 1998).The mechanism relies on the maintenance of pressure or a mechanical displacement of fluids. The most common secondary recovery method today is water injection, typically termed water-flooding, but gas injection is also used.

Tertiary recovery is often called “Enhanced Oil Recovery” or EOR for short.(Green and Willhite, 1998). This form of recovery affects the residual oil saturation to increase oil recovery. Tertiary processes can be CO_2, surfactant, polymer or low salinity injection. The common denominator is that they change the interaction between the injected fluid and the reservoir fluid.

3. Reservoir Characterization by tracers injection

Tracers are chemical substances that are applied in minor quantities in an oil recovery process in order to keep track of fluid flow, characterize the reservoir formation and eventually assist in the selection of optimal recovery strategies .They are ideally inert

compounds, which follow only the fluid under investigation. They are used widely by the oil industry for reservoir monitoring and improved reservoir description.

The aforementioned oil recovery and reservoir characterization technologies rely on the complicated interplay of a series of transport processes with the typically heterogeneous and anisotropy pore structure of petroleum reservoirs. These transport processes include both immiscible and miscible two-phase (oil-water) and three-phase (oil-water-gas) flows, hydrodynamic dispersion of tracers and dissolved species and energy transfer (mechanical and heat) over extended length scales. The rigorous numerical modeling of such processes at the pore and field scales is thus of crucial importance on the characterization of oil reservoirs and the development of novel oil recovery technologies. The modeling of such transport processes, typically encountered during secondary oil recovery, is the main objective of this thesis, as will be discussed in more detail below.

4. Objectives of this MSc thesis

Waterflooding and water-based floods are the most widely used secondary recovery methods. In cases where the water entering the field comes from many different sources, managing the waterfloods operation can become difficult. The addition of a tracer to the injected water is the only means of distinguishing between injection water and formation water, or between waters from different injection wells in the same field. Tracers are added to waterfloods for many reasons and in a variety of circumstances. (Zemel, 1995) They can be a powerful tool for describing the reservoir, investigating unexpected anomalies in flow, or verifying suspected geological barriers or flow channels. They can also be used in a test section of the field before expanding the flood. Flow in most reservoirs is anisotropic. The reservoir structures are usually layered and frequently contain significant heterogeneities leading to directional variations in the extent of flow. As a result, the manner in which water moves in the reservoir can be difficult to predict. Tracers are used in enhanced oil recovery pilot tests to monitor the actual water-flow pattern during the test. The ability to identify the water source is basic to the use of tracers for all the purposes described above. The tracer response as a function of position and time provides a qualitative description of fluid movement that can play a useful part in managing the flood and thus the recovery mechanism of the oil in a specific reservoir. These particular transport processes will be the main focus of this thesis. The objective is to offer better physical insight on how pore scale effects such as hydrodynamic dispersion determine the field scale transport properties in such upscaled systems. This will be accomplished using a commercially available generic finite element solver numerical modeling tools; Comsol Multiphysics. A comparison with the results with the numerical simulator Eclipse, which is widely used in the oil recovery industry, will be also attempted.

Chapter 2: Numerical modeling using Comsol Multiphysics.

Comsol Multiphysics is a powerful interactive environment used to model and solve all kinds of scientific and engineering problems. With this software conventional models for one type of physics can easily be extended into multiphysics models that solve coupled physics phenomena and do so simultaneously.

Using predefined Comsol's interfaces, it is possible to build models by defining the relevant physical quantities such as material properties, loads, constraints, sources, and fluxes rather than defining the underlying equations. The software internally compiles a set of equations representing the entire model through a flexible graphical user interface or by script programming in Java or the Matlab language.

Using these physics interfaces, you can perform various types of studies including:

• Stationary and time-dependent (transient) studies

• Linear and nonlinear studies

• Eigenfrequency, modal, and frequency response studies

When solving the models, Comsol assembles and solves the problem using a set of advanced numerical analysis tools. The software runs the analysis together with adaptive meshing and error control using a variety of numerical solvers. Furthermore creates sequences to record all steps that create the geometry, mesh, studies and solver settings, and visualization and results presentation. It is therefore easy to parameterize any part of the model with the use of the software's interface. The Software use Partial differential equations (PDEs) form the basis for the laws of science and provide the foundation for modeling a wide range of scientific and engineering phenomena.(COMSOL, 2013)

Finite Element Method theory

The Finite Element Method is a mathematical approach in which a continuum problem can be solved by dividing the solution domain into smaller spatial elements. These elements, termed as finite elements, have the same properties with the original equations, but they are simpler to define and to reduce the number of unknowns (Huebner, 2001).

The division results in elements composed by edges and nodes which are points of interception and connection between elements. The solution of differential equations regarding the physical problem can be solved by approximated functions that satisfy the conditions described by integral equations in the problem domain. These approximated functions are usually polynomial functions (Huebner, 2001).

In FEM there are two ways to solve problems described as partial differential equations. The so-called "strong form" is the direct resolution of the equations. The "weak form" has evolved from approximated numerical methods that are integral representations of differential equations governing the physical problem. The "strong form" requires continuity in the solution of dependent variables so it's more difficult to work with. The "weak form" allows a unique method to solve different types of problems because the methods to transform differential equations in an integral form are generics that usually provide more precise results. Due to its advantages in complex geometries it is the most used form (Liu, 2003).

The general steps of the Finite Element Method are described as follows:

The first step consists in the division of the body in small elements. The type, size and number of elements are in the field of the engineer judgment but can be supported with research. Next step is to choose interpolation functions. It is defined in the element using the nodal values of the element. The most common functions are linear, quadratic and cubic polynomials, because they are simple to work with. The degree of the polynomial varies according to the number and nature of nodes of the elements and the unknowns at each node. The following step is to set the matrix equations. For this, various methods can be used. In order to obtain the final and global equation for the system, the next step is to collect and assemble the equations for the element properties. Previously to solving the system of equations, the equations have to be changed so that it can regard the boundary conditions. The assemblage results in a group of equation with unknown nodal values, degrees of freedom. The kind of equations to be solved depends on the type of problem and if it is time dependent or not. In the end, other parameters dependent of those calculated can be also obtained. Those parameters are also referred as derived values and can be volume, surface averages or integrations or simply just point evaluation of certain quantities. (Huebner, 2001).

Chapter 3: Hydrodynamic dispersion in a single capillary

1. Introduction

The phenomenon of hydrodynamic dispersion occurs in problems of underground mixing of water of different quality in petroleum reservoirs during injection processes. In these problems, any identifiable solute may serve as a tracer whose concentration distribution indicates the mixing.

The nature of dispersion or miscible displacement in porous media may be examined from both an over-all, or macroscopic, and a local, or microscopic, view-point. Because of the complexities of the structure of such media, there are difficulties associated with both approaches. Overall behavior, such as the average concentration distribution at the system outlet as a function of time, can be observed in sets of experiments, as is frequently done in practice, and the results can be correlated with the variables investigated on empirical or semi empirical bases. The objective of this case study is to distinguish the progress made in one attempt to identify the mechanisms of dispersion and miscible displacement in a single capillary. Because the geometry of the microstructure is generally too complex to be described by a single model, a simplification is been made by examining the evolution of those phenomena in a pipe in order to simulate the effects occurring in a single pore. The medium is considered to consist of a microstructure made up of the pores and void spaces in and between the solid materials. This requires that the important mechanisms controlling the transport are identified through experiment so that realistic microstructure models may be developed.

To implement macroscopically correct laws for describing miscible displacements, knowledge of local behavior is required, since integral results which reflect overall behavior are obtained from integrating the differential equations which are assumed to describe local behavior. It is assumed that the microscopic equations of change are accurate enough to

describe phenomena as they occur in a porous medium. However, the application of these equations to porous media is difficult. Consider the flow boundaries in even the most orderly packed bed, and the geometric complexities are clear.

Finally, the microscopic results need to be combined and averaged so that a comparison with macroscopic behavior can be attained. At this point, the theory is intimately related to experiment since, it is necessary to compare experimental measurements with analytic solution in order to evaluate the quality of the results.

The model of dispersion in porous media, introduces a new mechanism of spreading of the tracer that is due to the different rates of advance of the tracer in capillaries of different orientations. This mechanism can bring about much greater spreading than Taylor's dispersion in individual capillary tubes.

The dispersion coefficient, which is a measure of the rate at which material will spread out axially in the system, is enhanced by having large differences in velocity exist across the flow and by taking place in equipment with large transverse dimensions. In contrast, any mechanism which increases transverse mixing, such as turbulence or transverse convection currents, reduces the dispersion coefficient. These arguments apply, in a qualitative way, to porous media as well as to simple configurations. That is, in porous media, dispersion is created by both the microscopic differences in velocity which exist in the interstices between particles and by large-scale or macroscopic effects such as channeling (Dullien, 1979; Nunge, and Gill, 1969).

2. Transport equations for Hydrodynamic Dispersion

Dispersion phenomena occur in many important fields of technology, for example, in petroleum reservoir engineering, ground water hydrology, chemical engineering, chromatography. A few examples are so called miscible flood in petroleum recovery; transition zone between salt waste disposal into acquifers; radio activate and ordinary sewage soil; packed reactors in chemical industry; use of various 'tracers' in petroleum engineering and hydrology research projects, etc.

The treatment of hydrodynamic dispersion is divided here in two main sections: Dispersion in a capillary tube and dispersion in a porous medium. The reasons for examining the dispersion process in a capillary are twofold. First, the phenomenological equations describing dispersion are often the same as in the case of a porous medium. Second, dispersion in a capillary tube, the mechanism of which is relatively well understood, plays a role in determining dispersion in porous media.

In this chapter the following process takes place; A solvent (water) is flowing in long capillary under steady state conditions at low Reynolds numbers. A second species (tracer) is completely dissolved in the flow stream to form a solution. The tracer concentration is spatially variable, but always at the dilute limit. Namely, the tracer concentration does not affect the bulk phase (solvent) properties. Therefore properties of solvent are the same as the properties of solution before the injection of the tracer.

The hydrodynamic dispersion process is then determined by the equations for the flow of the solution and the mass conservation of the diluted species.

Navier Stokes equation: Momentum Conservation

The Navier-Stokes equations govern the motion of fluids and can be seen as Newton's second law of motion for fluids. In the case of a compressible Newtonian fluid, this yields

$$\rho(\frac{\partial u}{\partial t} + u*\nabla u) = -\nabla p + \nabla*(\mu(\nabla u + (\nabla u)^T) - \frac{2}{3}\mu(\nabla*u)I) + \mathbf{F} \quad \textbf{\textit{(3.1.1)}}$$

Where **u** is the fluid velocity, **p** is the fluid pressure, **ρ** is the fluid density, and **μ** is the fluid dynamic viscosity. The different terms correspond to the inertial forces (first term), pressure forces (second), viscous forces (third), and the external forces applied to the fluid (forth). The Navier-Stokes equations were derived by Navier, Poisson, Saint-Venant, and Stokes between 1827 and 1845.

In the limit of low Reynolds numbers Re->0 and under steady state conditions, which is typically the case for pore media flows, the acceleration terms (on the left-hand of Eq.(**3.1.1**)) are negligible, and thus the above equation reduces to the Stokes equation;

$$\nabla p=\nabla*(\mu(\nabla u + (\nabla u)^T) - \frac{2}{3}\mu(\nabla*u)I) + \mathbf{F} \quad \textbf{\textit{(3.1.2)}}$$

These equations are always solved together with the continuity equation:

$$\frac{\partial \rho}{\partial t} + \nabla*(\rho \mathbf{u}) = 0 \quad \textbf{\textit{(3.2.1)}}$$

Equation **(3.2.1)** for the typical case of an incompressible fluid under steady state conditions reduces to:

$$\nabla*u=0 \quad \textbf{\textit{(3.2.2)}}$$

The Navier-Stokes (or Stokes) equations represent the conservation of momentum, while the continuity equation represents the conservation of mass for the solution (water and dissolved tracer).

Mass Balance Equation - Mass conservation of diluted species

The Transport of diluted species at the pore space is governed by diffusion and convection as described by the following equation:

$$\frac{\partial c}{\partial t} + \mathbf{u}\nabla c = \nabla*(D\nabla c) + R \quad \textbf{\textit{(3.3)}}$$

c is the concentration of the species (mol/m^3)

D denotes the diffusion coefficient (m^2/s)

R is a reaction rate expression for the species (mol/(m^3 ·s))

u is the velocity vector (m/s)

The first term on the left-hand side of Equation ***(3.3)*** corresponds to the accumulation of the species.

The second term accounts for the convective transport due to a velocity field u. This field can be expressed analytically or be obtained from coupling this physics interface to one that describes fluid flow (momentum balance). To include convection in the mass balance equation, an expression that includes the space and time variables, or the velocity vector component variable names from a fluid flow physics interface of Comsol, can be entered into the appropriate field. The velocity fields from existing fluid flow interfaces are available directly as predefined fields (model inputs) for multiphysics couplings.

On the right-hand side of the mass balance equation ***(3.3.1)***, the first term describes the diffusive transport, accounting for the interaction between the dilute species and the solvent. A field for the diffusion coefficient is available, and any expression containing other variables such as pressure and temperature can be entered here. The node has a matrix that can be used to describe anisotropic diffusion coefficients.

Finally, the second term on the right-hand side of Equation ***(3.3.1);*** represents a source or sink term, typically due to a chemical reaction. In order for the chemical reaction to be specified, another node must be added to Comsol's Transport of Diluted Species interface the Reaction node, which has a field for specifying a reaction equation using the variable names of all participating species. (COMSOL Multiphysics 2015)

Dispersion in a single Capillary

The simplest model for characterizing the microstructure in porous materials is the straight tube. Bundles of straight capillaries have long been used to model flow through porous media and assemblages of randomly oriented straight pores or capillaries, where it is assumed that the path of a marked element consists of a sequence of statistically independent steps, direction and duration of which vary in a random manner. Here the results of capillary dispersion are considered for the purpose of illustrating the interactions of some of the factors influencing dispersion in porous media. The straight tube provides a well-defined hydrodynamical system where the dispersion process is most easily described while still retaining many of the main features of the same process in porous media.

Consider first the dispersion of two fluids of the same constant physical properties in a straight capillary tube with steady fully developed laminar flow prevailing. An early experimental work which demonstrated the essence of the process without mathematical treatment was reported by Griffiths in 1911, who observed that a tracer injected into a stream of water spreads out in a symmetrical manner about a plane in the cross section which moves with the mean speed of flow. This is a rather startling result for two reasons. First, since the water near the center of the tube moves with twice the mean speed of flow and the tracer at the mean speed, the water near the center must approach the column of tracer, absorb the tracer as it passes through the column, and then reject the tracer as it leaves on the other side of the column. Second, although the velocity is unsymmetrical about the plane moving at the mean speed, the column of tracer spreads out symmetrically. The concentration of the tracer material is described by the two-dimensional unsteady convective diffusion equation, equation ***(3.4).***

$$\frac{\partial c}{\partial t} + u(r)\frac{\partial c}{\partial x} = Ð\left(\frac{\partial^2 c}{\partial x^2} + \frac{1}{r}\frac{\partial}{\partial r} r \frac{\partial c}{\partial r}\right) \quad \textbf{(3.4)}$$

Here C is the point concentration, u the parabolic laminar velocity profile, and x and r the axial and radial coordinates, respectively. Taylor showed that for a large enough number of times the process could be described by a one-dimensional dispersion model, as given in equation ***(3.5).***

$$\frac{\partial \hat{c}}{\partial t} + \bar{u}\frac{\partial \hat{c}}{\partial x} = D_{ct}\frac{\partial^2 \hat{c}}{\partial x^2} \quad \textbf{(3.5)}$$

Upon defining a coordinate which moves with the mean speed of flow as:

$$x' = x - \bar{u}t \quad \textbf{(3.6)}$$

Equation ***(3.5)*** becomes

$$\frac{\partial \hat{c}}{\partial t} = D_{ct}\frac{\partial^2 \hat{c}}{\partial x'^2} \quad \textbf{(3.7)}$$

The above equation is simply the one-dimensional unsteady diffusion equation to which solutions are readily available under a variety of conditions. The molecular diffusion coefficient has been replaced by an effective axial diffusion coefficient or dispersion coefficient which, in the absence of axial molecular diffusion, Taylor showed to be

$$K = \frac{4a^2 {u_m}^2}{192D} \quad \textbf{(3.8.1)}$$

$$K = D_{ct} \quad \textbf{(3.8.2)}$$

Where α is the tube radius. This simple equation provides a great deal of physical insight into the nature of the dispersion process if we interpret the numerator to be a measure of axial convection and the denominator to reflect the intensity of transverse mixing rather than just transverse molecular diffusion.

The solution of the ***(3.5)*** equation, known as second law of diffusion, is well known for the case under consideration:

$$\frac{\hat{C}}{C_o} = \frac{1}{2(\pi * Dct * t)}\exp\left[-\frac{(x - \bar{u} * t)^2}{4Dct * t}\right] \quad \textbf{(3.6)}$$

Where c_0 is the initial tracer concentration in the slug and $D_{ct}=\sigma_x^2/2t$, with σ_x the standard deviation of the Gaussian distribution of the tracer concentration. Therefore, the length of the mixed zone in Figure 1 keeps increasing symmetrically on both sides of the tracer concentration maximum in the middle of the slug. The concentration tapers off to zero at both ends of the slug.

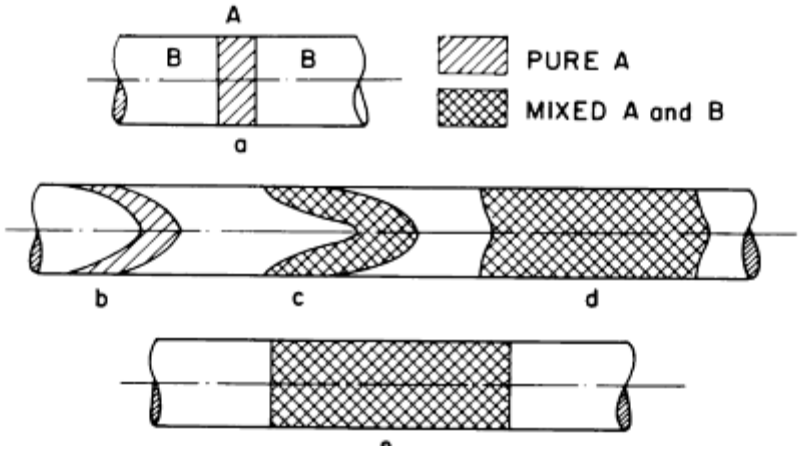

Figure 1: Schematic representation of the mixed zone for A dispersing in B as function of time [Dullien, 1979]

In this event, we see that the dispersion coefficient, which is a measure of the rate at which material will spread out axially in the system, is enhanced by having large differences in velocity exist across the flow and by taking place in equipment with large transverse dimensions. In contrast, any mechanism which increases transverse mixing, such as turbulence or transverse convection currents, reduces the dispersion coefficient. These arguments apply, in a qualitative way, to porous media as well as to simple configurations. That is, in porous media, dispersion is created by both the microscopic differences in velocity which exist in the interstices between particles and by large-scale or macroscopic effects such as channeling. Aris later extended the analysis to include axial molecular diffusion and demonstrated that the dispersion coefficient for this case contains Taylor's result with an additive term due to diffusion. (Dullien, 1979)

$$k = D + \frac{4a^2 * Um^2}{192D} \quad \textbf{(3.7)}$$

This combined result will be referred to as the Taylor-Aris theory. It is important to note the restriction placed on the Taylor-Aris theory with respect to time, since, unless this time is exceeded, the mean concentration distribution is not described by a dispersion model. For porous media, the dimension in the flow direction must be large enough to ensure sufficient residence time for a dispersion model to apply.

The formal analogy of Equation ***(3.6)*** with Fick's second law of diffusion may easily lead to the false conclusion that in hydrodynamic dispersion the driving force of spreading of the tracer is the axial concentration gradient $\partial c_{average} / \partial x'$, which in the reality is a result of an interplay between axial convection and radial diffusion. In other words is the effect rather than the cause of the process.

For the case of negligible axial molecular diffusion, Taylor showed D_{ct} to be given as

$$D_{ct} = R^2 \bar{u}^2 / 48 Ð = Pe_{ct}^2 Ð / 192 \quad \textbf{(3.8)}$$

Where D_{ct} includes the effect of both mechanical and (or convective) dispersion and radial molecular diffusion. It is enlightening to note that as $Ð \rightarrow \infty$, $D_{ct} \rightarrow 0$ and as $Ð \rightarrow 0$, $D_{ct} \rightarrow \infty$.

Hence, very intense radial mixing eliminates dispersion and the absence of radial mixing results in a infinite dispersion coefficient.

Aris (1956), however, showed that when the axial molecular diffusion is not negligible, the axial dispersion coefficient contains an additive term due to diffusion.

$$D_{ct} = Ð + R^2 \bar{u}^2/48\, Ð = Ð + (Pe_{ct}^2/192) \quad \textbf{(3.9)}$$

Inspection of Equations ***(3.8)*** and ***(3.9)*** shows that the rate of spreading (dispersion) increases rapidly with tube diameter and velocity, and it decreases with increasing diffusion coefficient, at least as long as $\mathbf{R^2\, \bar{u}^2/48\, Ð}$ is much greater than Ð. (Dullien, 1979)

3. Model Implementation in Comsol Multiphysics

In the following case study, the Navier-Stokes equations and the mass conservation equation are numerically solved in a computational domain, such as the one shown in Figure 2. In order for those equations to be implemented in Comsol multiphysics two interfaces where utilized, namely Laminar flow interface and Transport of diluted species interface. Furthermore, the differential equations need to be solved with a set of boundary conditions. At the next figure the 2D Axisymmetric Pipe Flow geometry is illustrated.

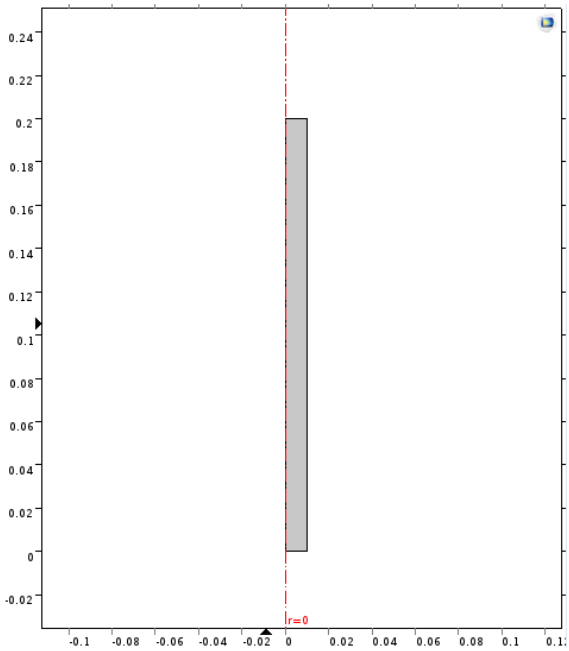

Figure 2: Axisymmetric Pipe flow, Capillary Dimensions (Height 0.2, Width 0.01 m)

Laminar flow interface

Pressure is specified as 1e5+0.0005 Pa at the inlet and as 1e5 Pa at the outlet. A no-slip boundary condition (i.e., the velocity is set to zero) is specified at the side walls of the capillary. The numerical solution of the steady-state NS (the time-dependent derivative is set to zero) and continuity equations in the laminar regime and for constant boundary conditions.

Transport of diluted species interface

Convection acts as an additional transport mechanism. Moreover the average velocity from the laminar flow interface is set as an input to the mass conservation of diluted species equation. Diffusion coefficient is isotropic and selected as 5e-8[m^2/s]. No flux boundaries (-$\mathbf{n}*\mathbf{N}_i$=0) are set at the side walls of the capillary and as initial concentration 0 mol/m^3 is selected. As an inflow boundary a time dependent concentration is implemented 5*flc2hs(t[s^-1]-20,0.1)-5*flc2hs(t[s^-1]-22,0.1).

Laminar flow interface is solved as a stationary problem and Transport of diluted species as a time dependent one with a range of (0, 0.5, 2400) second. The two equations are coupled and aim to identify the hydrodynamic dispersion coefficient D_{ct}. The results that are extracted with the use of the above Comsol multiphysics model are illustrated next.

4. Results & Discussion

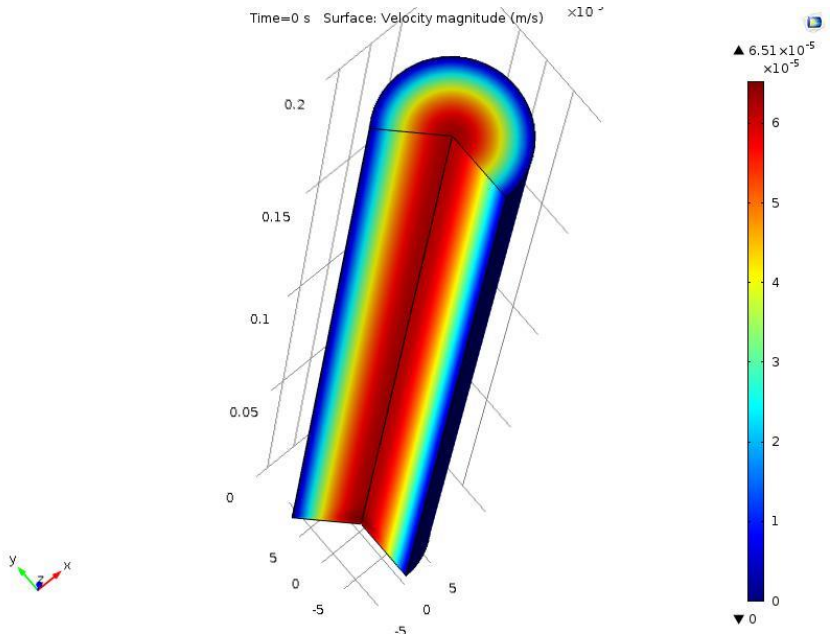

Figure 3: Velocity magnitude (parabolic) in the case of the axisymmetric pipe (Peclet number 12.24)

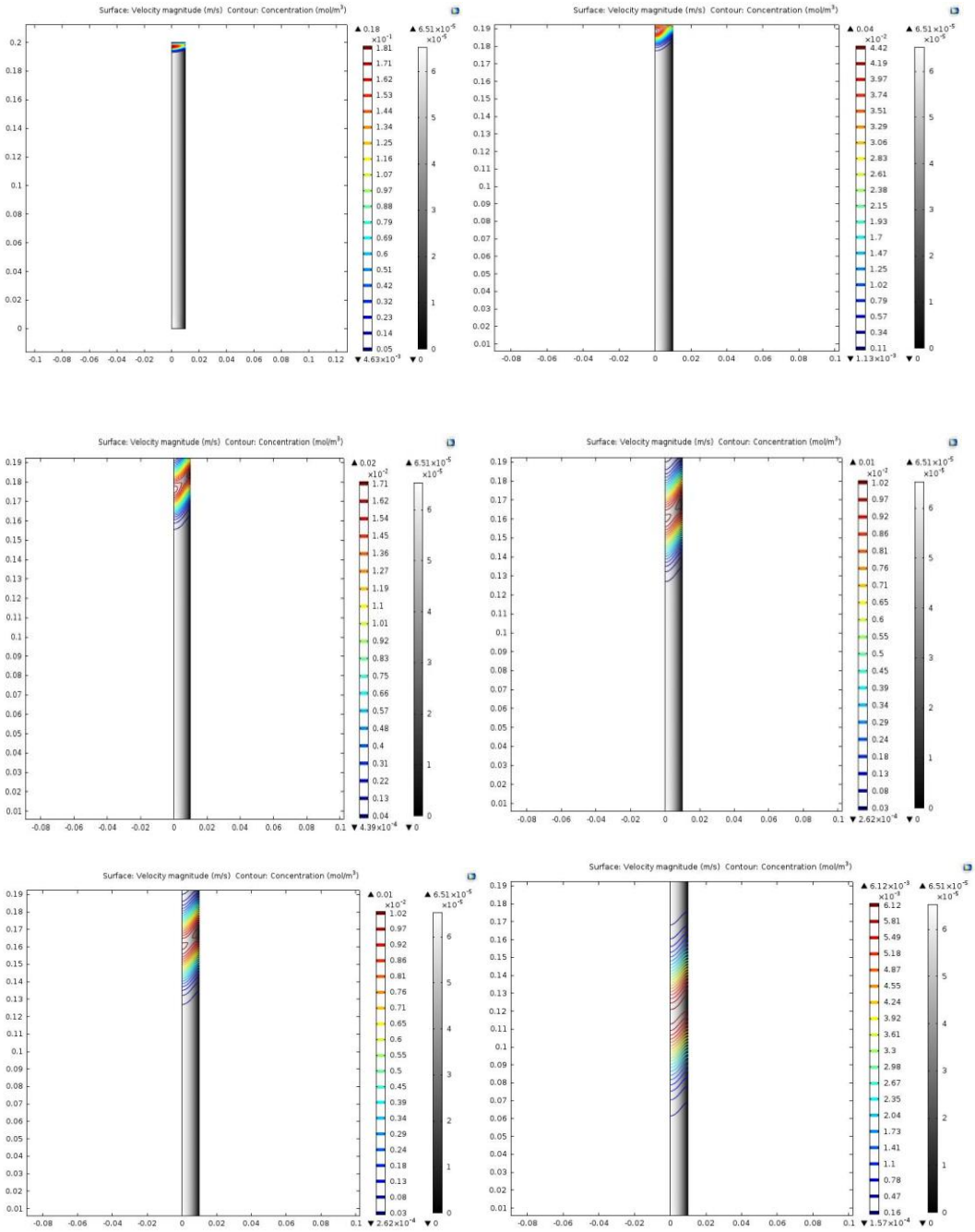

Figure 4. Parabolic concentration profile for the tracer; at 50, 200, 500,1000,1800,2400 sec. (Peclet 12.42)

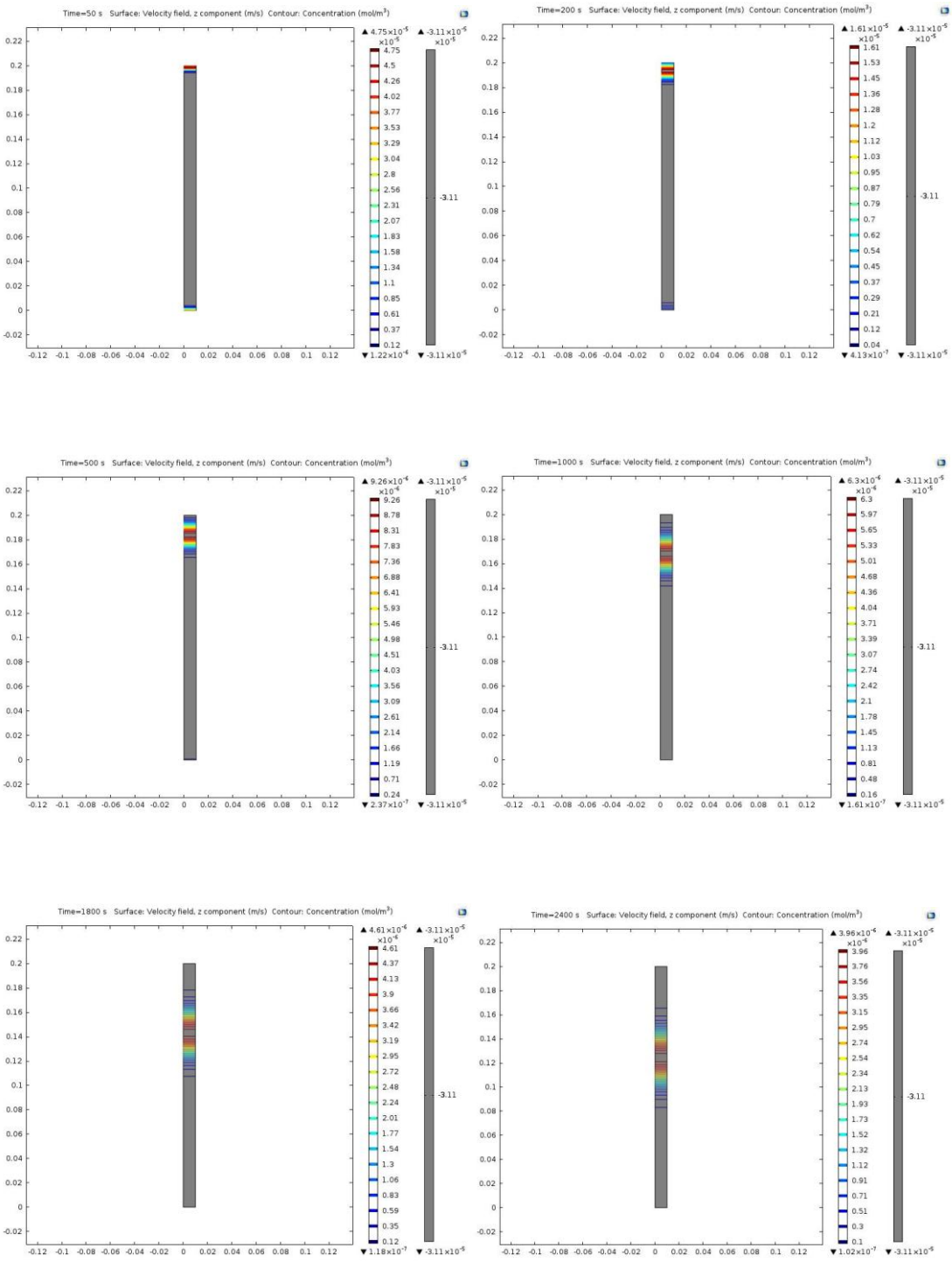

Figure 5: Flat concentration profile for the tracer; at 50, 200, 500, 1000, 1800, 2400 sec. (Peclet 12.42)

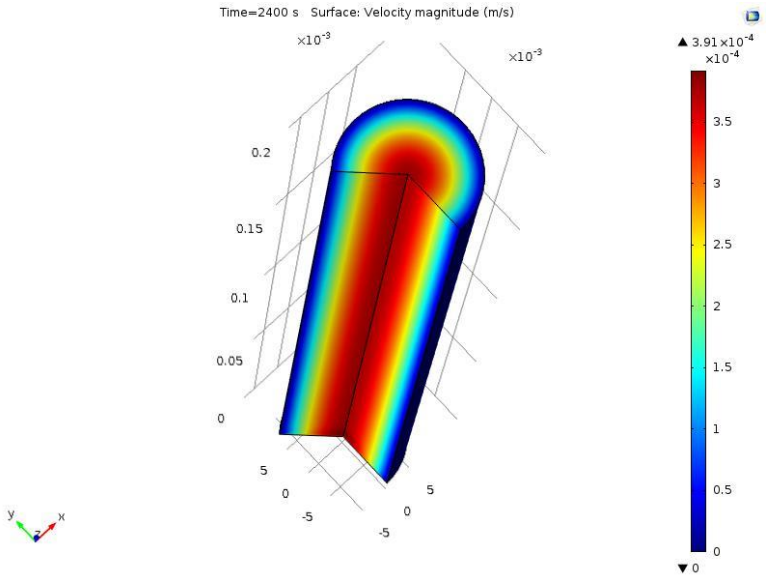

Figure 6: Velocity magnitude (parabolic) in the case of the axisymmetric pipe. (Peclet 24.86)

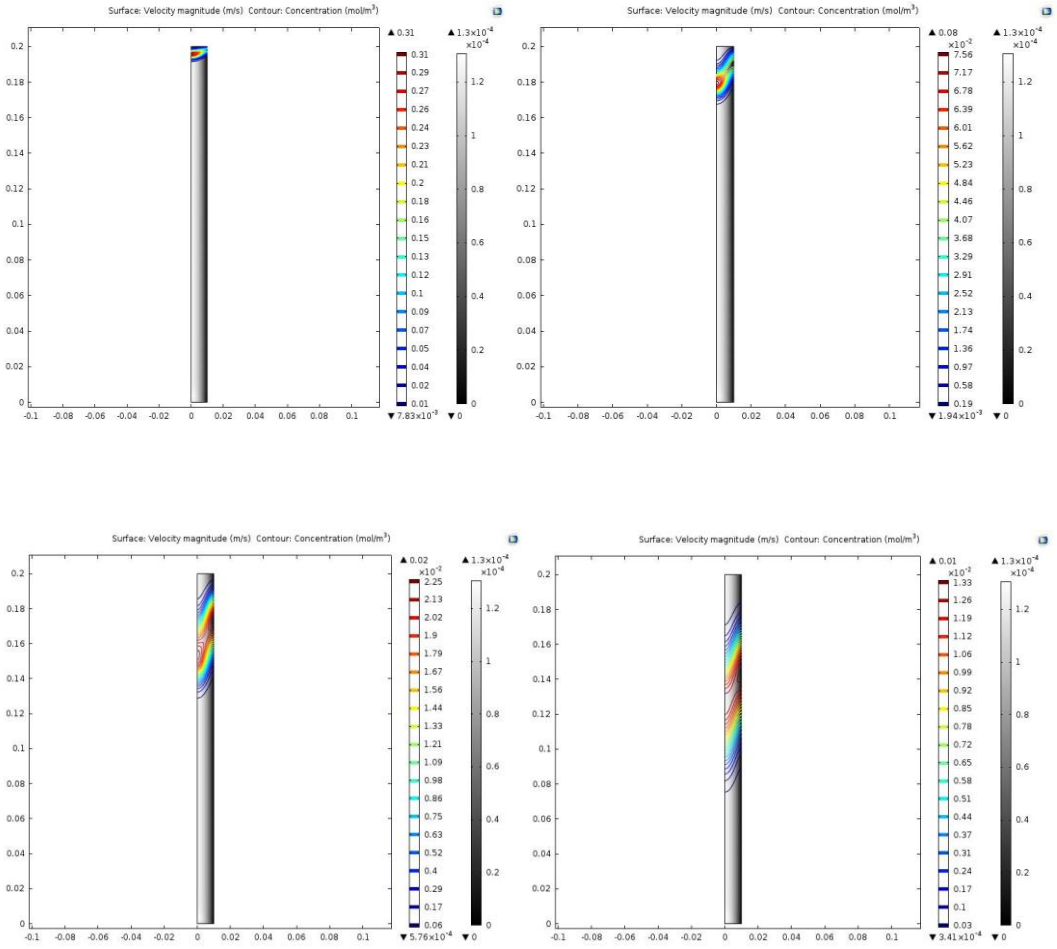

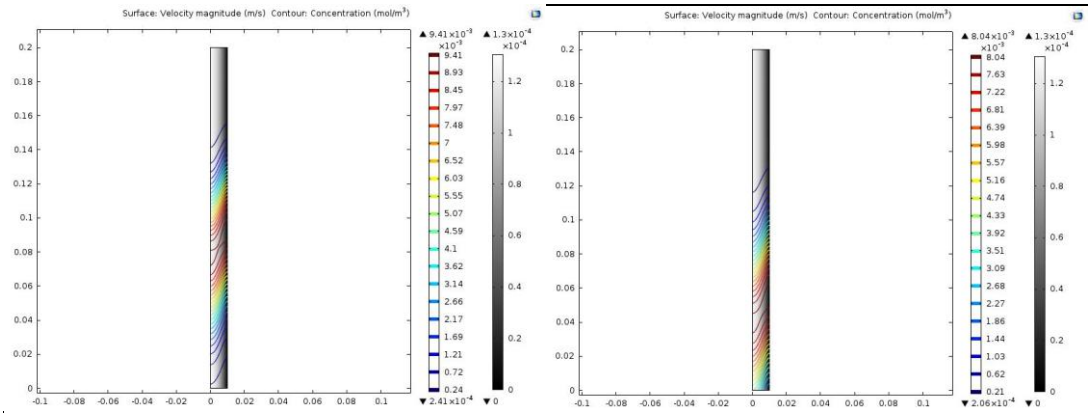

Figure 7: Parabolic concentration profile for the tracer; at 50, 200, 500, 1000, 1800, 2400 sec. (Peclet 24.86)

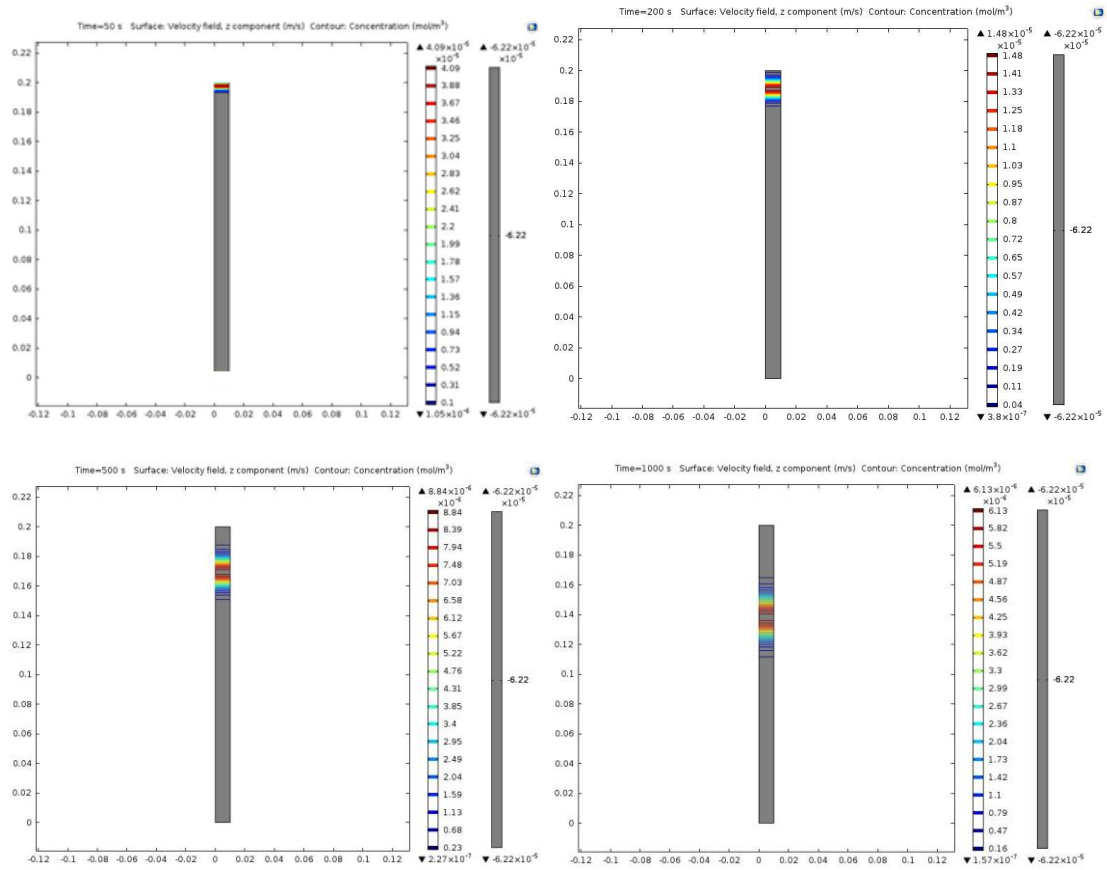

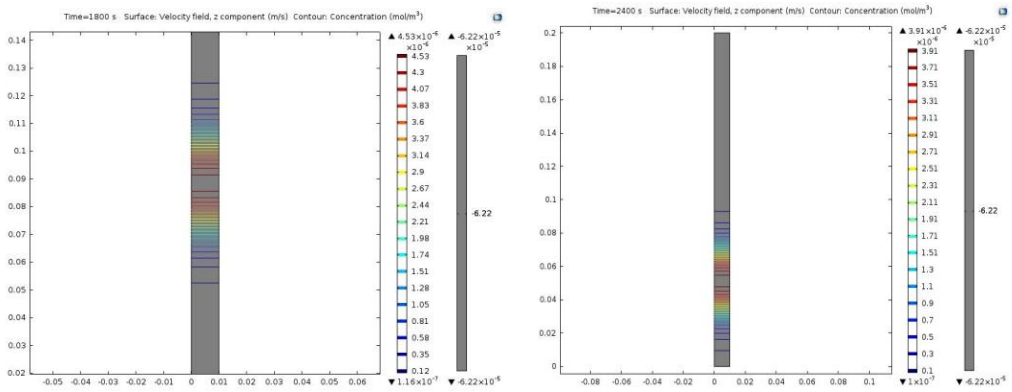

Figure 8: Flat concentration profile for the tracer; at 50, 200, 500, 1000, 1800, 2400 sec.(Peclet 24.86)

Velocity profile (Parabola-Flat)

The solution of the NS equation in a such a capillary yields a parabolic velocity profile with an analytical solution described by Eq.***(3.10).*** This particular velocity profile significantly enhances the mixing of diluted species in the direction parallel to the flow due to the development of concentration gradients in the transverse direction. These combined effected lead to longitudinal (in the flow direction) dispersion coefficients that are always higher that the molecular diffusion coefficient and a function of the Peclet number as discussed above.

Neglecting the exact velocity profile at the pore scale, as is typically the case in field (Darcy) scale modeling essentially leads to the assumption of a flat (piston-like) velocity profile at the pore scale where the dispersion coefficient is always equal to molecular diffusivity. In the case, therefore, of Darcy scale modeling the exact values for the dispersion coefficient tensor should be given as input, being previously evaluated either experimentally or using rigorous pore scale modeling.

The effects of pore scale velocity profiles are thus discussed below. Equations describing Paraboloid and Flat velocity of the flow acting inside the capillary:

Paraboloid velocity

$$u(r)= \left(\frac{R^2-r^2}{4\mu}\right)\frac{\Delta P}{L} \qquad \textbf{(3.10)}$$

Flat velocity

$$u(r)= \frac{R^2}{8\mu}\frac{\Delta P}{L} \qquad \textbf{(3.11)}$$

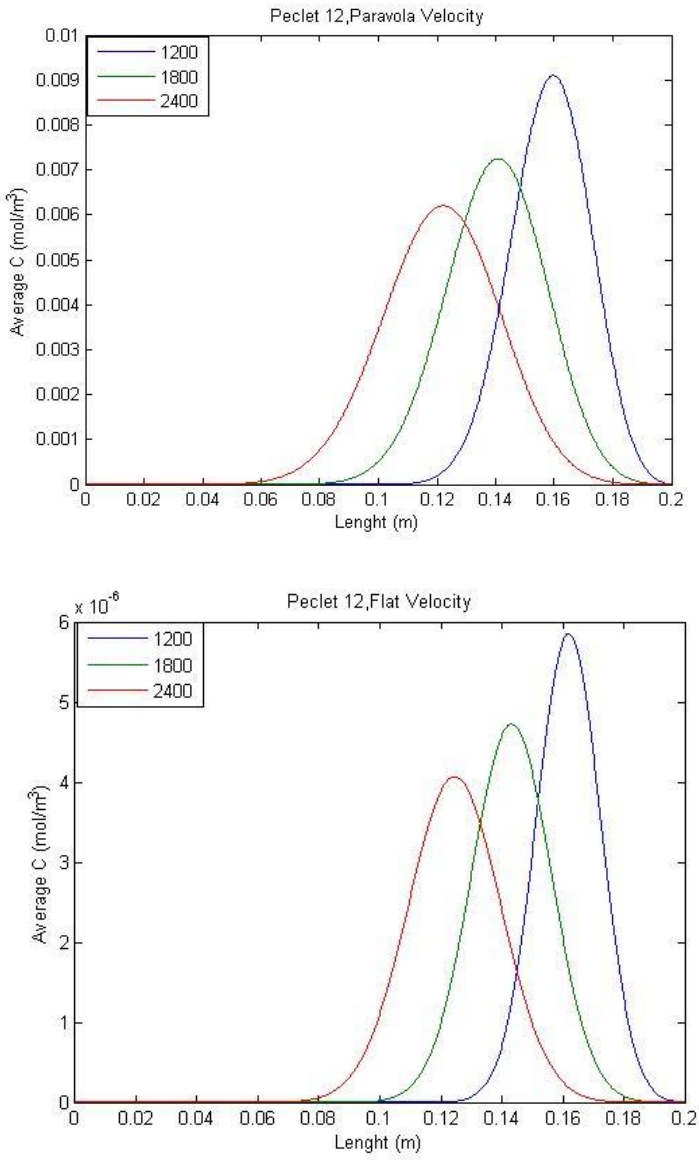

Figure 9: Comparison of the concentration profile of flat and parabolic velocity with the use of the 12.42 Peclet number

Figure 9 shows the average tracer concentration along the principal axis of the capillary at different times after tracer injection and for the two velocity profiles. The tracer injection follows a smooth Dirac delta function and takes place at the x=0.2m at a specified time step. The tracer is then carried towards the exit of the capillary (locate at x=0) under the flow of the solvent. It can be observed in the above figure, that the tracer concentration spreads with time, following however a Gaussian (normal) distribution with increasing variance for both velocity profiles. As expected the overall mass, calculated by integrated these curves in along the capillary axis, remains the same during all times.

For the case of the parabolic velocity profile, it is obvious that when the Peclet number is increasing, the variance of the Gaussian distribution is taking to higher values. Since $Dct=\sigma_\chi^2/2t$ and if equation ***(3.9)*** is taken into consideration it can be distinct that Dct is proportional to the square of the Peclet number.

A graphical summary of the regions of applicability of various analytical solutions for dispersion for the step change in inlet concentration has been given by Nunge and Gill (1969) ***(Figure 11)*** with the $\tau=t\text{Đ}/R^2$ and the Peclet number $Pe_{ct}=2R\bar{u}/\text{Đ}$ as parameters. An important point is relating to the dispersion model is that τ must be sufficient large for it to apply. For example 0.8 for fully developed laminar flow in tubes.

The comparison between the concentration distributions for the two velocity profiles reveals that, while the average position of the distribution is the same in both cases, the variance increases more rapidly in the case of the parabolic velocity profile, demonstrating the important effects of microscale velocity on hydrodynamic dispersion.

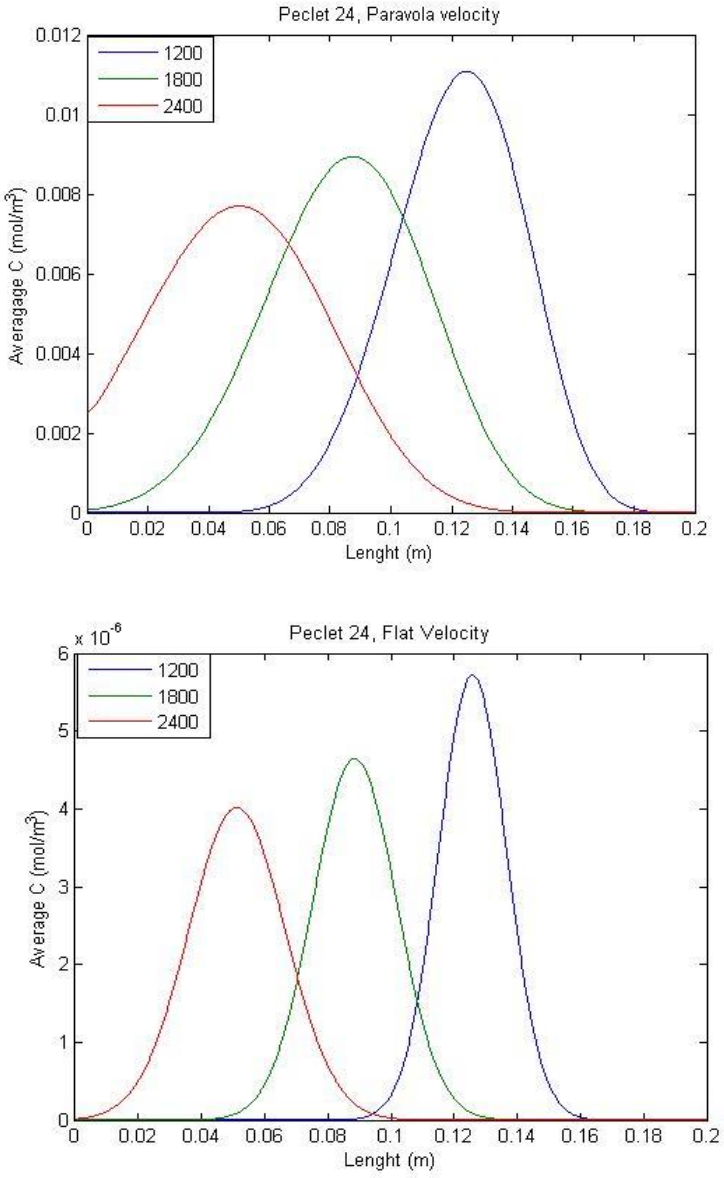

Figure 10: Comparison of the concentration profile of the parabolic and flat velocity with the use of 24.86 Peclet number

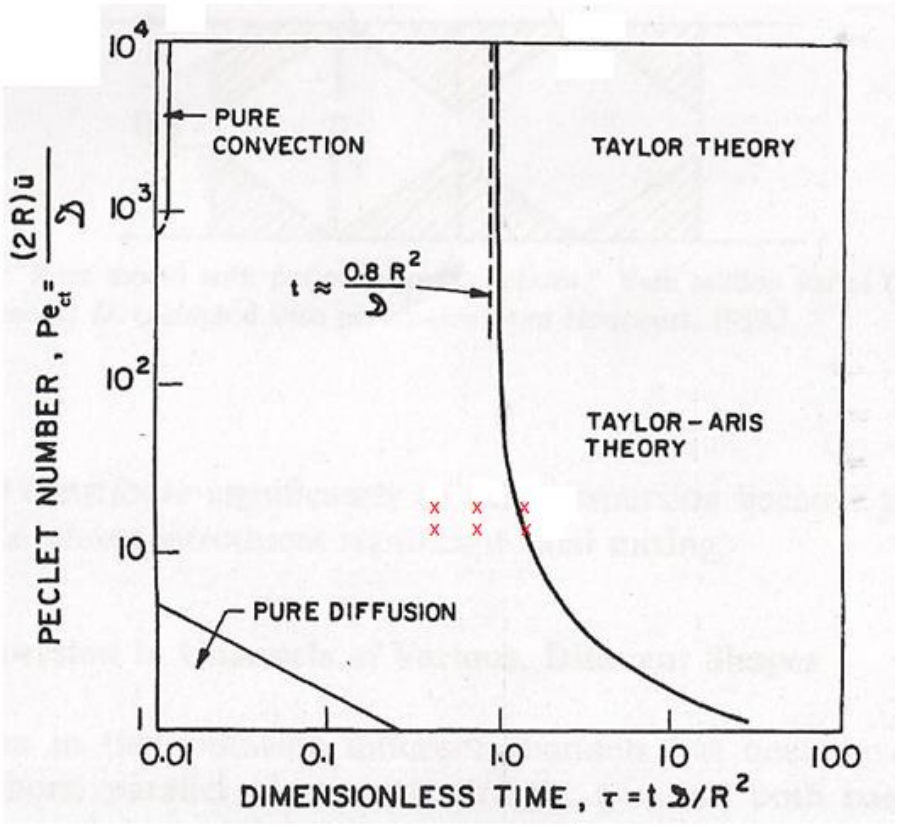

Figure 11: Summary of the regions of applicability of various analytical solutions for dispersion in capillary tubes with a step change in inlet concentration as a function of τα and Pe_{ct}. [Dullien, 1979]

At high Peclet numbers with the same fluids, a straight channel having the same equivalent diameter (four times the hydraulic radius) as a tube requires a minimum real time of approximately 1/3 of that for the tube before the dispersion model applies, thus indicating that the minimum real time requirement is a strong function of the geometry of the system.

The Concentration profiles of figures 9 & 10 were used as an input in the curve fitting tool of Matlab. Standard deviation of each Gaussian profile was computed as a next step. Since the coefficient of hydrodynamic dispersion follows the $D_{ct}=\sigma^2/2*t$ formulation, where t is the time that slug disperse in the stream of water, three specific times were selected in each case for the calculation of D_{ct}. Dimensionless time ($\tau = t*D/R^2$) also is computed for 1200, 1800, 2400 sec and the results are presented in the next table. The analytic solution which is used for verification is $D_{ct} = 9.02*10^{-8}$ m^2/s.

Parabolic Velocity Profile			Flat Velocity Profile		
Peclet	12.43	Dimensionless	Peclet	12.43	Dimensionless
Time	$D_{ct}(10^{-8}\ m^2/s)$	Time (τ)	Time	$D_{ct}(10^{-8}\ m^2/s)$	Time (τ)
1200	7,79	0,6	1200	4,64	0,6
1800	8,17	0,9	1800	4,75	0,9
2400	8,37	1,2	2400	4,81	1,2
Parabolic Velocity Profile			Flat Velocity Profile		
Peclet	24.86	Dimensionless	Peclet	24.86	Dimensionless
Time	$D_{ct}(10^{-7}\ m^2/s)$	Time (τ)	Time	$D_{ct}(10^{-8}\ m^2/s)$	Time (τ)
1200	1,97	0,6	1200	4,85	0,6
1800	2,02	0,9	1800	4,9	0,9
2400	2	1,2	2400	4,92	1,2

Table 1: Hydrodynamic dispersion coefficient for different times and Peclet numbers with parabolic and flat velocity profiles in a capillary

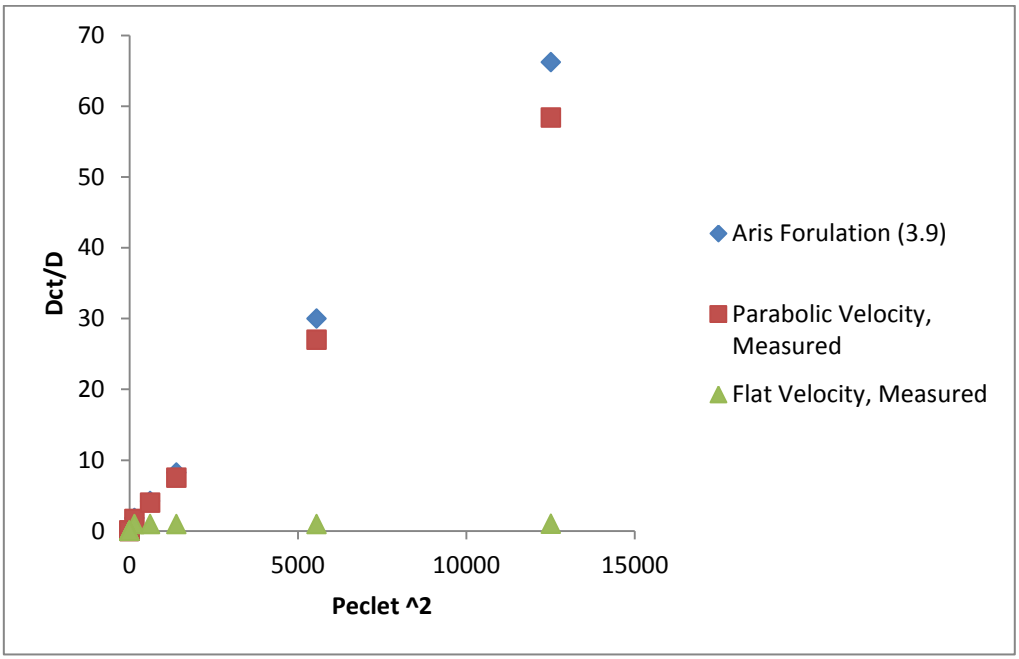

Figure 12: Hydrodynamic dispersion coefficient variance, at different Peclet numbers

In figure 12, hydrodynamic dispersion coefficient is presented for three different cases. The blue dots refer to ***(3.9)*** formulation, illustrating the analytic solution of hydrodynamic dispersion as it was introduced by Aris. It is obvious that for the case of parabolic velocity, numerical modeling provides an adequate match with Aris formulation. A deviation can be identified in the last case of 112 Peclet number, which is an expected result since from various experiments conducted the region of applicability for hydrodynamic dispersion is from zero to 100 Peclet number. In the case of Flat velocity profile, as it was studied for the same Peclet number as in the case of paraboloid, hydrodynamic dispersion coefficient remains constant despite the fact that Peclet number is keep increasing. The above result supports the argument that the driving force of hydrodynamic dispersion, and thus the

driving force of the hydrodynamic mixing, is the parabolic profile of the velocity as it was indicated from the results extracted from this chapter.

5. Conclusion of chapter 3

In this chapter a numerical model was implemented in Comsol multiphysics in order to study hydrodynamic dispersion in a single capillary. Microscale effects that arise in a single capillary are a simplification of the effects taking place at the pore scale. The purpose for this study was to explicitly calculate the Dispersion coefficients (D_{ct}) and evaluate its dependence on the Peclet number for various flow regimes. It is evident from the results extracted from this part of the thesis, which for parabolic velocity profiles, such as those typically encountered in actual pore structures; hydrodynamic dispersion is a function of the Peclet number. On the contrary, when the velocity profile is flat, the Dispersion coefficient remains independent of Pe and equal to the molecular diffusivity of the species. To conclude, an accurate knowledge of the velocity profile at the pore scale is necessary for the precise calculation of reservoir transport properties such as the Dispersion Coefficient (D_{ct}).

Chapter 4: Modeling Hydrodynamic Dispersion at the field scale

1. Introduction

The detailed structure of a porous medium is greatly irregular and just some statistical properties are known. An exact solution to characterize flowing fluid through one of these structures is basically impossible. For this reason, modeling hydrodynamic dispersion at the field scale has profound differences with modeling in a single capillary as presented in the previous chapter. The precise pore scale velocity profile is not known a priori, as is in the case for dispersion in a single capillary (where it was parabolic rather than flat). Not knowing this information we need to rely on experimental results and the derived semiempirical models to derive values for the dispersion tensor. In this chapter this information cannot be calculated as previously. Instead it is provided as an input assuming a volume averaged (upscaled over several pore volumes) velocity profile, typically expressed through Darcy's equation, rather than the actual micro (pore) scale profile as before. Using the method of volume or spatial averaging it is possible to obtain the transport equation for the average concentration of solute in a porous medium (Bear, 1972).

The usefulness of water flood tracers is based upon the assumption that the movement of the tracer reflects the movement of the injected water. How closely this holds true depends upon how closely the tracer follows the injected water through a formation without significant loss or delay. This in turn depends upon how well the chemical composition of the tracer meets the constraints set by the properties of the formation. Radioactive isotopes are used to tag chemical tracers to provide analytical tools of high selectivity and sensitivity. The tracer properties, however, are defined only by their chemical composition. In this case study a hydrodynamic dispersion coefficient value is implemented as an input in the model in order to provide information about pore behavior of the diluted specie.(Zemel, 1995)

Firstly the direction of flow from the injector towards the producer can be identified. Furthermore the parts of the reservoir where the total velocity is greater can be distinct. The overall behavior of the reservoir is verified with the use of the dispersion of the tracer in three dimensions. The macroscopic results are linked with the pore behavior that was presented at chapter three. The only difference in this chapter is that dispersion takes place in three dimensions and in order for this behavior to be quantify longitudinal and transverse dispersion (parallel and vertical to the direction of flow) are predefined. When the model is set and verified, contour plots are illustrates to provide information about the behavior of the tracer during the injection of water in the life of the reservoir. Normal total flux that is removed from the reservoir in various times is plotted as well. Moreover the total quantity of mol that exists in the reservoir at each time step is presented in order to identify the influence of stratified geometry in the model. Finally a contrast is illustrated between two cases of stratified reservoirs; heterogeneous and homogeneous anisotropic three layered cases for the Normal total flux (mol/s) and for the Ntotal (mol) existing in the reservoir.

A three dimensional model is implemented in this chapter in order to simulate the mass transfer of a tracer under the single phase flow of water in a stratified petroleum reservoir. Prediction of macroscopic transport properties of a porous medium from its geometric characteristics (e.g. porosity, stratified geometry) is investigated in this case study. Conservation of momentum in the form of Darcy's law equation is used to simulate single phase flow in porous media. Conservation of mass of diluted species at the field scale is simulated with the use of Comsol's Diluted Species interface.

2. Transport equations for Hydrodynamic dispersion in porous media

In the case of saturated flow through a porous medium, if in a portion of the flow domain a certain mass of solute is inserted; this solute will referred as a tracer. Various experiments indicate that as flow takes place the tracer gradually spreads and occupies an ever-increasing portion of the flow domain, beyond the region it is expected to occupy according to the average flow alone. This phenomenon is called hydrodynamic dispersion in a porous medium. It is a non-steady, irreversible process in which the tracer mass mixes with the liquid solute. If initially the tracer-labelled liquid occupies a separate region, with an abrupt change separating it from the unlabeled liquid, this interface does not remain an abrupt one, the location of which may be determined by the average velocity expressed by Darcy's Law. (Bear, 1972)

In general, hydrodynamic dispersion consists of two parts: mechanical dispersion and molecular diffusion. Mechanical dispersion results from the movement of individual fluid particles which travel at variable velocities through tortuous pore channels of the porous medium. The complicated system of interconnected passages comprising the microstructure of the medium cause a continue subdivision of the tracer's mass into finer offshoots. Variation in local velocity, both in magnitude and direction along the tortuous flow paths and between adjacent flow paths are result of the velocity distribution within each pore. The random fluid movement in irregular flow paths generates a blended region between the two fluids. The amount of spreading depends on the dispersive capability of the porous medium. The property of porous medium that is a measure of its capacity to cause mechanical

dispersion is called dispersivity. In general, dispersivity is considered to have two components: one in the direction of mean flow (longitudinal dispersion) and one perpendicular to the direction of mean flow (transverse dispersion). For practical purposes, however, transverse dispersion has a minor effect on the amount of mixing between fluids compared to longitudinal dispersion. (Bear, 1972; Bear & Bachmat, 1967; Maghsood & Brigham, 1982)

The second component of hydrodynamic dispersion, molecular diffusion occurs on a macroscopic level as a consequence of net concentration gradients across surfaces perpendicular to the average flow direction. It is caused by the random movement of the differing molecules. This molecular diffusion contributes to the growth of the mixed region as well.

Darcy's Equation for momentum transfer in porous media

Darcy's law equation is actually the momentum conservation equation in this chapter. It can be derived from the Navier Stokes using volume averaging. The presence of spatial deviations of the pressure and velocity in the volume-averaged equations of motion gives rise to representation for the spatial deviations are derived that lead to Darcy's law.

In a porous medium, the global transport of momentum by shear stresses within the fluid is typically negligible; because the pore walls impede momentum transport to the fluid outside the individual pores (namely friction with the pore walls is dominant over friction between adjacent fluid layers). A detailed description, down to the resolution of every pore, is not practical in most applications. A homogenization of the porous and fluid media into a single medium is a common alternative approach. Darcy's law together with the continuity equation and equation of state for the pore fluid (or gas) provide a complete mathematical model suitable for a wide variety of applications involving porous media flows, for which the pressure gradient is the major driving force.

Darcy's equation describes fluid movement through interstices in a porous medium. Because the fluid loses considerable energy to frictional resistance within pores, flow velocities in porous media are very low. The Darcy's Law interface in the Subsurface Flow Module applies to water moving in an aquifer or stream bank, oil migrating to a well. Also set up multiple Darcy's Law interfaces to model multiphase flows involving more than one mobile phase.

Darcy's law portrays flow in porous media driven by gradients in the hydraulic potential field, which has units of pressure. For many applications it is convenient to represent the total hydraulic potential or the pressure and the gravitational components with equivalent heights of fluid or head. Division of potential by the fluid weight can simplify modeling because units of length make it straightforward to compare to many physical data. The physics interface also supports specifying boundary conditions and result evaluation using hydraulic head and pressure head. In the physics interface, pressure is always the dependent variable. Darcy's law applies when the gradient in hydraulic potential drives fluid movement in the porous medium. Visualize the hydraulic potential field by considering the difference in both pressure and elevation potential from the start to the end points of the flow line. According to Darcy's law, the net flux across a face of porous surface is

$$\mathbf{u} = -\frac{k}{\mu}(\nabla p + \rho g \nabla D) \qquad \textit{(4.1)}$$

In this equation, u is the Darcy velocity or specific discharge vector (m/s); κ is the permeability of the porous medium (m^2); μ is the fluid's dynamic viscosity (Pa·s); p is the fluid's pressure (Pa) and ρ is its density (kg/m^3); g is the magnitude of gravitational acceleration (m/s^2); and ∇D is a unit vector in the direction over which the gravity acts. Here the permeability, κ, represents the resistance to flow over a representative volume consisting of many solid grains and pores. (COMSOL, 2013).

Transport of Diluted Species in Porous Media

The following equations for the concentrations, c_i, describe the transport of solutes in a variably saturated porous medium for the most general case, when the pore space is primarily filled with liquid but also contain pockets or immobile gas:

$$\frac{\partial}{\partial t}(\theta c_i) + \frac{\partial}{\partial t}(\rho_b c_{P,i}) + \frac{\partial}{\partial t}(a_v C_{G,i}) + \mathbf{u}*\nabla c_i = \nabla*[(D_{D,I} + D_{e,I})\nabla c_i] + R_i + S_i$$

(4.2)

On the left-hand side of the above equation, the first three terms correspond to the accumulation of species within the liquid, solid, and gas phases, while the last term describes the convection due to the velocity field u (m/s).

c_i denotes the concentration of species i in the liquid (mol/m^3), $c_{P,i}$ the amount adsorbed to (or desorbed from) solid particles (moles per unit dry weight of the solid), and $c_{G,i}$ the concentration of species i in the gas phase.

The equation balances the mass transport throughout the porous medium using the porosity ε_p, the liquid volume fraction θ; the bulk (or drained) density, $\rho_b = (1 - \varepsilon_p)\rho$, and the solid phase density ρ (kg/m^3).

For saturated porous media, the liquid volume fraction θ is equal to the porosity ε_p, but for partially saturated porous media, they are related by the saturation s as $\theta = s\varepsilon_p$. The resulting gas volume fraction is $a_v = \varepsilon_p - \theta = (1\text{-}s)\varepsilon_p$.

On the right-hand side of Equation ***(4.2)***, the first term introduces the spreading of species due to mechanical mixing (dispersion) as well as from diffusion and volatilization to the gas phase. The tensor is denoted D_D (m^2/s) and the effective diffusion by D_e (m^2/s).

The last two terms on the right-hand side of Equation ***(4.2)*** describe production or consumption of the species; R_i is a reaction rate expression which can account for reactions in the liquid, solid, or gas phase, and S_i is an arbitrary source term, for example due to a fluid flow source or sink.

n order to solve for the solute concentration of species i, c_i, the solute mass sorbed to solids $c_{P,i}$ and dissolved in the gas-phase $c_{G,i}$ are assumed to be functions of c_i.(COMSOL, 2013).

Convective Term Formulation

The Transport of Diluted Species in Porous Media interface includes two formulations of the convective term. The conservative formulation of the species equations in Equation ***(4.2)*** as described before.

If the conservative formulation is expanded using the chain rule, then one of the terms from the convection part, $c_i \nabla \cdot u$, would equal zero for an incompressible fluid and would result in the non-conservative formulation described in Equation ***(4.2).***

When using the non-conservative formulation, which is the default, the fluid is assumed incompressible and divergence free: $\nabla \cdot u = 0$. The non-conservative formulation improves the stability of systems coupled to a momentum equation (fluid flow equation). (COMSOL, 2013).

The velocity field to be used in the Model Inputs section on the physics interface can, for example, be prescribed using the velocity field from a Darcy's Law Equation interface.

The average linear fluid velocities u_a, provides an estimate of the fluid velocity within the pores:

$$u_a = \frac{u}{\varepsilon p} \quad \text{Saturated} \qquad \textbf{(4.3)}$$

$$u_a = \frac{u}{\theta} \quad \text{Partially saturated} \qquad \textbf{(4.4)}$$

Where ε_p is the porosity and $\theta = s*\varepsilon_p$ the liquid volume fraction, and S the saturation, a dimensionless number between 0 and 1.

Figure 13: A block of a porous medium consisting of solids and the pore space between the solid grains. [COMSOL, 2013]

The average linear velocity describes how fast the fluid moves within the pores. The Darcy's velocity attributes this flow over the entire fluid-solid face. (COMSOL, 2013)

Effective Diffusivity

The effective diffusion in porous media, D_e, depends on the structure of the porous material and the phases involved. Depending on the transport of diluted species occurs in free flow, saturated or partially saturated porous media, the effective diffusivity is defined as:

$$D_e = \frac{\varepsilon p}{\tau L} D_L \quad \textbf{(4.5)}$$

For a saturated Porous Media

Here D_L is the single-phase diffusion coefficients for the species diluted in pure liquid (m^2/s), and τ_L is the corresponding tortuosity factor (dimensionless).

The tortuosity factor accounts for the reduced diffusivity due to the fact that the solid grains impede the Brownian motion. The interface provides predefined expressions to compute the tortuosity factors according to the Millington and Quirk model. For a saturated porous media $\theta = \varepsilon_p$. The fluid tortuosity for the Millington and Quirk model that was used in the case study is the one presented below. (COMSOL, 2013)

$$\tau_F = \varepsilon_p^{-1/3} \quad \textbf{(4.6)}$$

Calculation of the Dispersion Tensor

The contribution of dispersion to the mixing of species typically overshadows the contribution from molecular diffusion, except when the fluid velocity is very small.

The spreading of mass, as species travel through a porous medium is caused by several contributing effects. Local variations in fluid velocity lead to mechanical mixing referred to as dispersion. Dispersion occurs because the fluid in the pore space flows around solid particles, so the velocity field varies within pore channels. The spreading in the direction parallel to the flow, or longitudinal dispersivity, typically exceeds the transverse dispersivity from up to an order of magnitude. Being driven by the concentration gradient alone, molecular diffusion is small relative to the mechanical dispersion, except at very low fluid velocities.

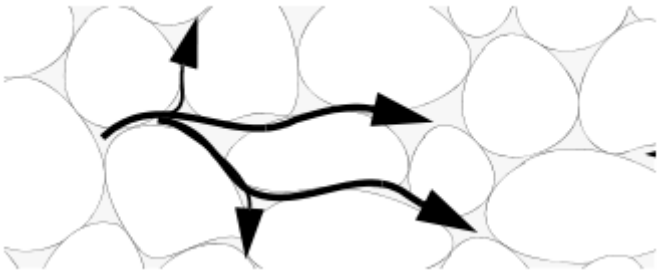

Figure 14: Spreading of fluid around solid particles in a porous medium [COMSOL, 2013]

Dispersion is controlled through the dispersion tensor D_D . The tensor components can either be given by user-defined values or expressions, or derived from the directional dispersivities.

Using the longitudinal and transverse dispersivities in 2D, the dispersion tensor components are (Bear, 1979):

$$D_{Dii} = a_L \frac{u_i^2}{|\mathbf{u}|} + a_T \frac{u_j^2}{|\mathbf{u}|} \quad (4.7.1)$$

$$D_{Dij} = (a_L - a_T) \frac{u_i u_j}{|\mathbf{u}|} \quad (4.7.2)$$

In these equations, D_{Dii} (SI unit: m^2/s) are the principal components of the dispersion tensor, and D_{Dji} and D_{Dji} are the cross terms. The parameters α L and α T (SI unit: m) specify the longitudinal and transverse dispersivities; and u_i (SI unit: m/s) stands for the velocity field components.

In order to facilitate modeling of stratified porous media in three dimensions, the tensor formulation by Burnett and Frind can be used. Consider a transverse isotropic media, where the strata are piled up in the z direction, the dispersion tensor components are:

$$D_{Lxx} = a_1 \frac{u^2}{|\mathbf{u}|} + a_2 \frac{v^2}{|\mathbf{u}|} + a_3 \frac{w^2}{|\mathbf{u}|} \quad (4.8.1)$$

$$D_{Lyy} = a_1 \frac{v^2}{|\mathbf{u}|} + a_2 \frac{u^2}{|\mathbf{u}|} + a_3 \frac{w^2}{|\mathbf{u}|} \quad (4.8.2)$$

$$D_{Lzz} = a_1 \frac{w^2}{|\mathbf{u}|} + a_2 \frac{u^2}{|\mathbf{u}|} + a_3 \frac{v^2}{|\mathbf{u}|} \quad (4.8.3)$$

$$D_{Lxy} = D_{Lyx} (a_1 - a_2) \frac{u v}{|\mathbf{u}|} \quad (4.8.4)$$

$$D_{Lxz} = D_{Lzx} (a_1 - a_3) \frac{u w}{|\mathbf{u}|} \quad (4.8.5)$$

$$D_{Lyz} = D_{Lzy} (a_1 - a_3) \frac{v w}{|\mathbf{u}|} \quad (4.8.6)$$

In the Equations above the fluid velocities u, v, and w correspond to the components of the velocity field u in the x, y, and z directions, respectively, and α_1 (m) is the longitudinal dispersivity. If z is the vertical axis, α_2 and α_3 are the dispersivities in the transverse horizontal and transverse vertical directions, respectively (m). Setting $\alpha_2 = \alpha_3$ gives the expressions for isotropic media shown in Bear (Bear, 1972; Bear, 1979).

3. Model Implementation in Comsol Multiphysics

In the second case study, Darcy's law and the mass conservation equations are numerically solved in a computational domain. In order for those equations to be implemented in Comsol multiphysics two interfaces where utilized; Darcy's Law and Transport of diluted species in porous media interfaces. Furthermore, these differential equations need to be solved together with a set of boundary conditions.

In the study section Darcy's Law interface is selected as a stationary problem and transport of diluted species in Porous media interface is selected as a time dependent problem for the solver to handle. The time units that where selected for the time dependent part of the

study are days and the range of the time variation is selected to be range(0,7,4368) days. The Solver configuration will start computing from time 0 until 4368 days with the use of time step of seven days.

As a first step to build the model in Comsol Multiphysics the geometry of the 3D porous media is implemented, as shown in Figure 15.

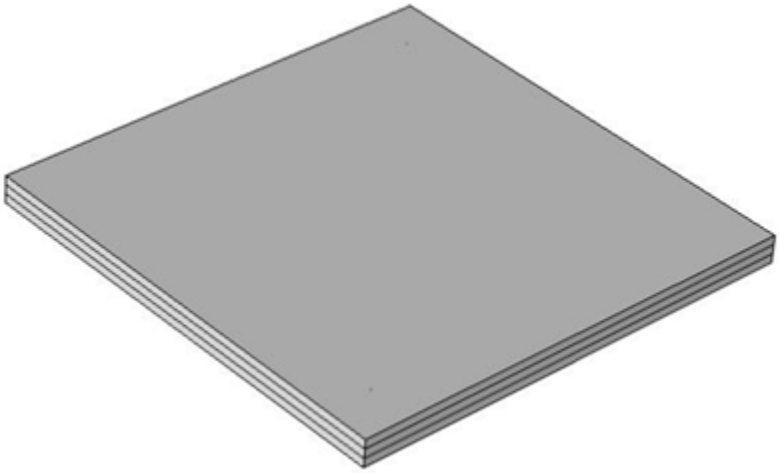

Figure 15: Geometry of the single phase flow reservoir

From the above figure it can be distinct that the reservoir is divided in three layers of equal thickness and different permeability. The three dimensional reservoir that was tailored has a size of 2500'x2500'x150'. Moreover in the reservoir presented above, two Wells are introduced; each one placed near an edge of the square geometry of the model. Each well is a cylinder with a radius of 0.67 ft and a height of 150 ft, equal with the perforations length. The mechanism than controls the system is the mass transfer of the water from the first well, which act as an injection well, towards the second well, which act as a production well.

Permeability (mD)	Top Layer	Middle Layer	Bottom Layer
X direction	200	1000	200
Y direction	150	800	150
Z direction	20	100	20

Table 2: Permeability in x, y, z direction in the three layers of the reservoir

Three domains are defined in Comsol model in order for the above anisotropic permeability values to be implemented. The value of 0.2 of porosity is also inserted in the matrix properties of each domain. As a next step of the procedure, initial value of 0 Pa is also defined in the Darcy's Law interphase. No flow boundaries ($-\mathbf{n}*\rho\mathbf{u} = 0$) are set in every wall of the reservoir at the side and at the top and the bottom of the stratified geometry. The inlet value of the injection well is set constant at $3.522*10^{-4}$ m/s. The outlet of the reservoir is defined with the use of pressure as 1000[kg/m^3]*9.81[m/s^2]*(150*0.3[m]-z) + 1e5[Pa].

As a second study step (time dependent) the transport of diluted species in Porous media interphase is introduced. The equations that were used in transport of diluted species interphase are presented below.

The difference in the equations that Comsol utilizes from the general ones is that no quantity of gas is present in porous media and the single phase fluid is considered to be incompressible. Furthermore $P_{1,j}$ and $P_{2,j}$ coefficients are functions of ε_p.

$$P_{1,j}\frac{\partial ci}{\partial t} + P_{2,j} + \nabla * \boldsymbol{\Gamma}_i + \mathbf{u} * \nabla c_i = R_i + S_i \qquad \textit{(4.9)}$$

$$P_{1,j} = \varepsilon_p \qquad \textit{(4.10)}$$

$$P_{2,j} = ci\frac{\partial \varepsilon p}{\partial t} \qquad \textit{(4.11)}$$

$$\mathbf{N}_i = \boldsymbol{\Gamma}_i + \mathbf{u}c_i = -(D_{D,j} + D_{e,j})\nabla c_i + \mathbf{u}c_i \qquad \textit{(4.12)}$$

Transport of diluted species in porous media equations, implemented by the interface of Comsol.

All three domains were selected and porosity value of 0.2 is selected for one more time in this interphase. Fluid diffusion coefficient of $D_{F,c2} = 9*10^{-9}$ m^2/s is defined and Millington & Quick model is selected for the description of Tortuosity.

In order for the contribution of dispersion to the mixing of species to be introduced an isotropic model was selected and the longitudinal and transverse dispersivity were set to 0.005 and 0.001 m respectively (COMSOL Multiphysics 2015). As initial value of concentration zero (mol/m^3) was selected. As an inflow the injection well walls were selected and a time dependent value of 20*flc2hs(t[d^-1]-2,1)-20*flc2hs(t[d^-1]-10,1) mol/m^3 is set.

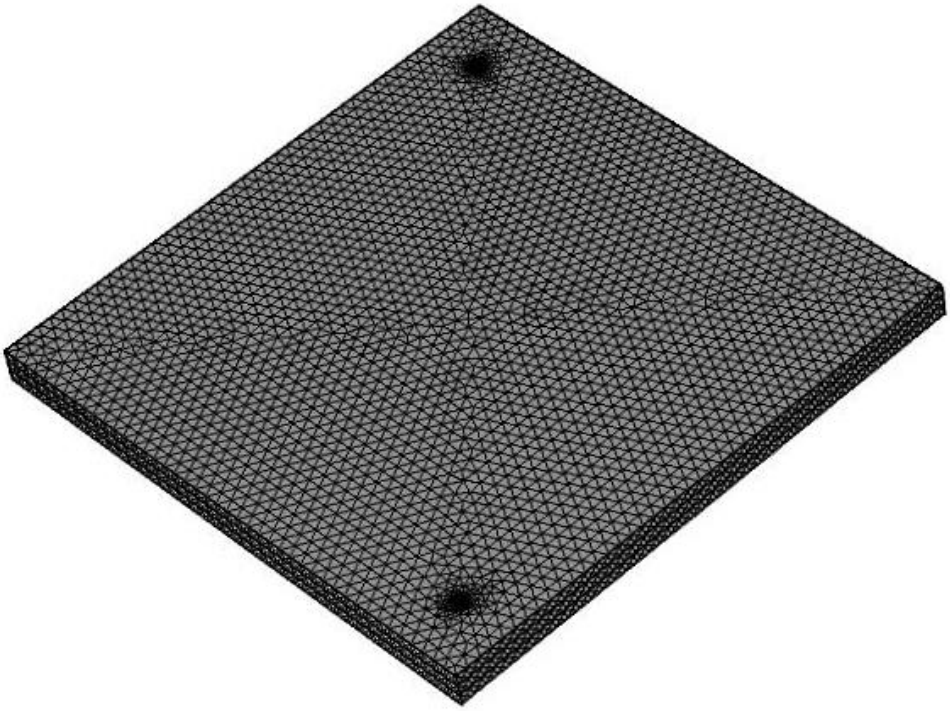

Figure 16: Extra fine element size- Mesh selected in 3D geometry model

The above mesh sequence physics control option was selected and the size of the element was selected to be extra fine. It is obvious that in the area around the wells the element size is even finer in order for the simulation to be more detailed in those areas.

4. Results & Discussion

In the figures below results are presented for the velocity field in order to ensure that model's results are physically correct. Firstly the direction of flow from the injector towards the producer can be identified. Furthermore the parts of the reservoir where the total velocity is greater can be distinct. The second layer produces longer arrows and this is due to the greater permeability of the second layer. Moreover the Size of the arrows is greater near the edges (producer, injector) where the reservoir is narrower and smaller in the middle where the reservoir is wider.

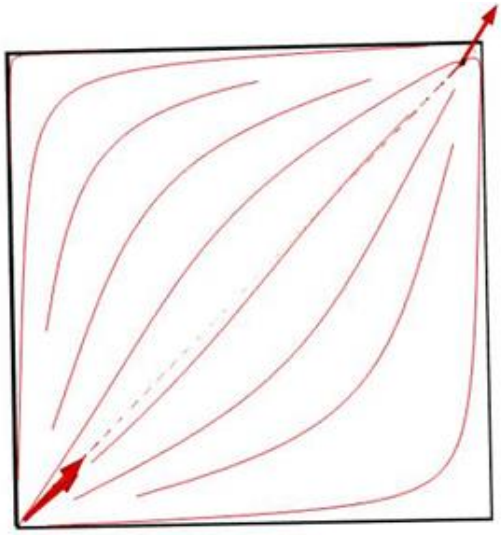

Figure 17: Top view of arrows and streamlines, representing velocity field

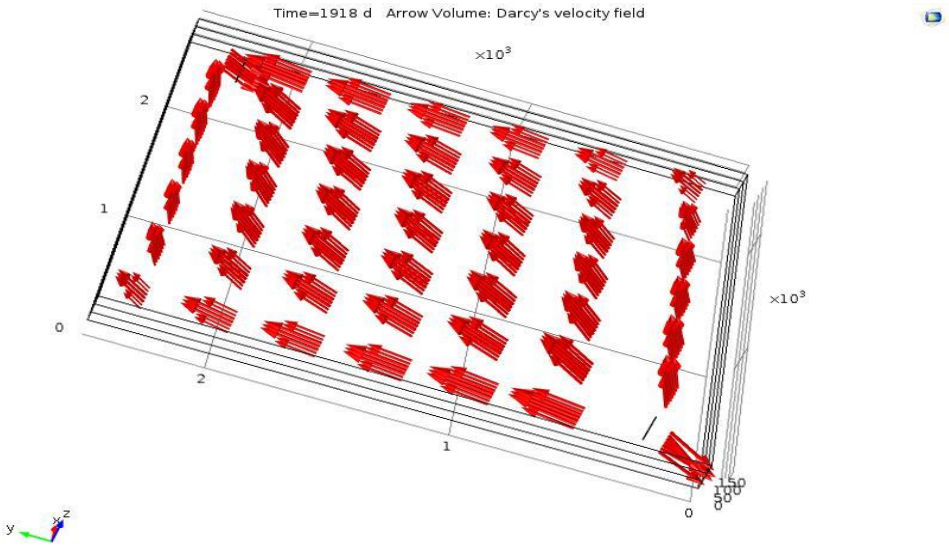

Figure 18: Side view of arrows representing velocity field

The two interphases (Darcy's Law, Transport of diluted species in porous media) where coupled and the profile of the concentration in 3 dimensions geometry in various times is presented below; for the tracer behavior to be distinguished.

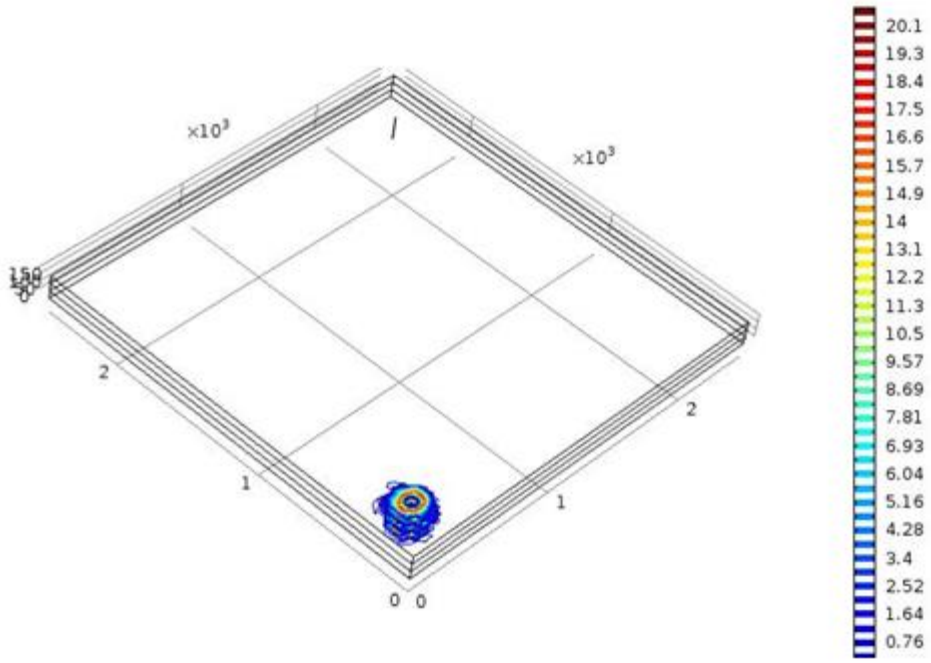

Figure 19: Contour concentration 3D graph; 14th day of tracer's injection

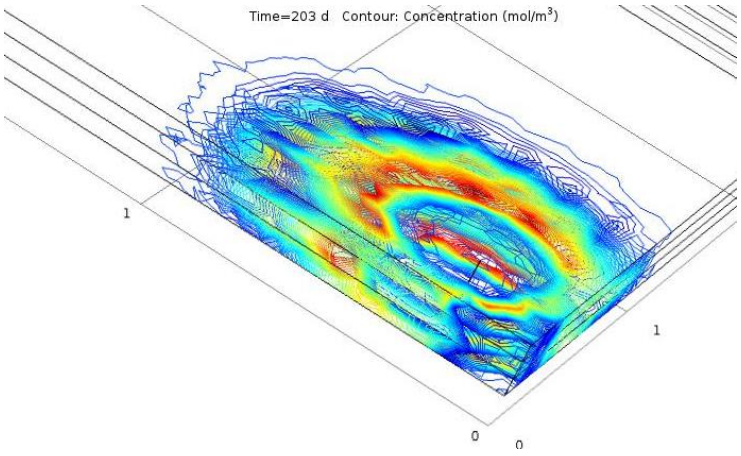

Figure 20: Injection well view at 203rd day of injection.

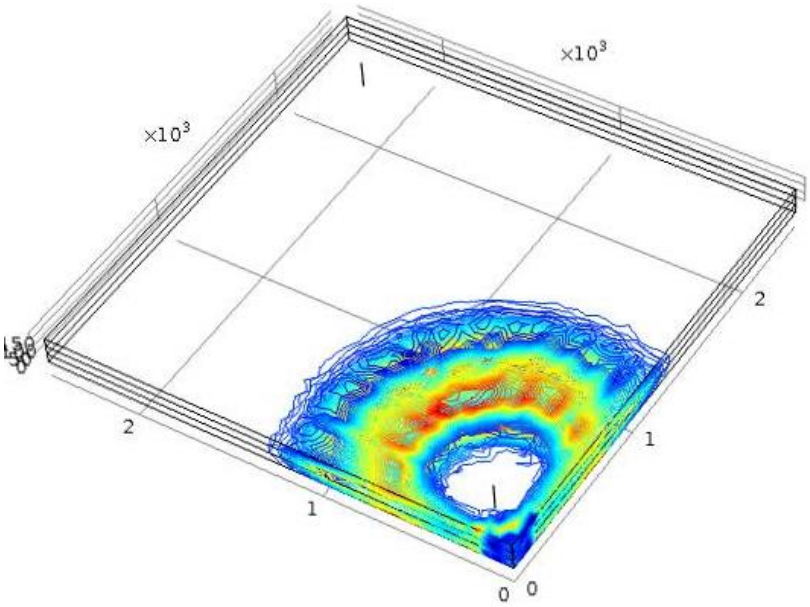

Figure 21: Contour concentration 3D graph; 364th day of tracer's injection

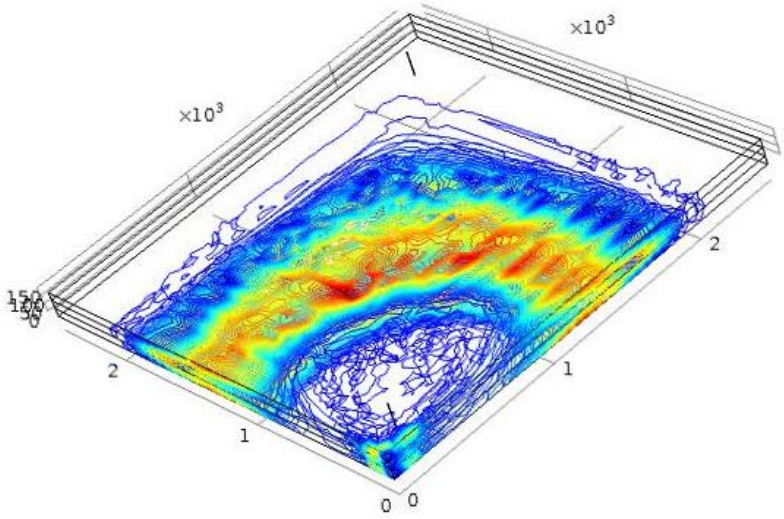

Figure 22: Contour concentration 3D graph; 1001st day of tracer's injection

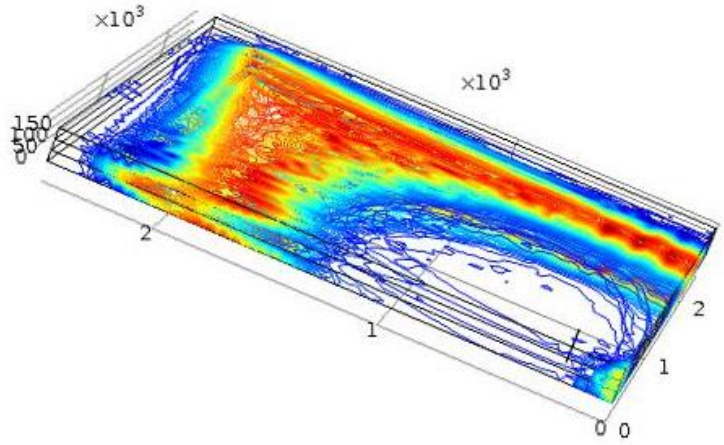

Figure 23: Contour concentration 3D graph; 2002nd day of tracer's injection

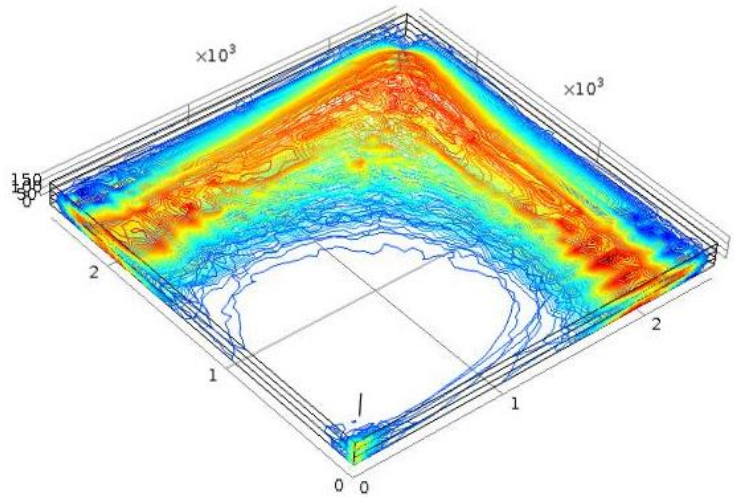

Figure 24: Contour concentration 3D graph; 2506th day of tracer's injection

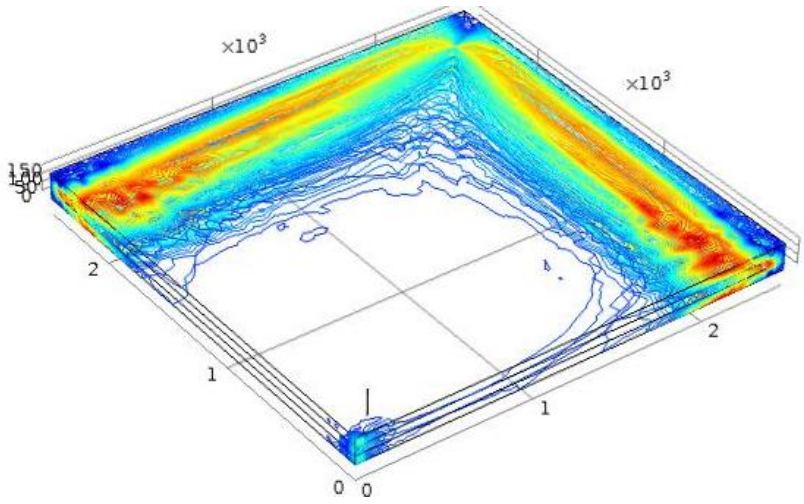

Figure 25: Contour concentration 3D graph; 3500 day of tracer's injection

The behavior of the tracer concentration profile in three dimensions provides adequate information about the model as well as for the tracer. The spreading of the tracer is more intense and takes place faster in the second layer due to its higher permeability. The spreading of the tracer also takes place in a greater extend in the bottom layer than the top one even though they have the same values of permeability in every direction, due to the effects of gravity through the hydrostatic pressure.

A comparison is also attempted with an identical model but with the same value of permeability in every layer in order to examine the influence of the medium heterogeneity on tracer spreading. In order to achieve that, a comparison of the spreading of the tracer at three different times after tracer injection is illustrated below.

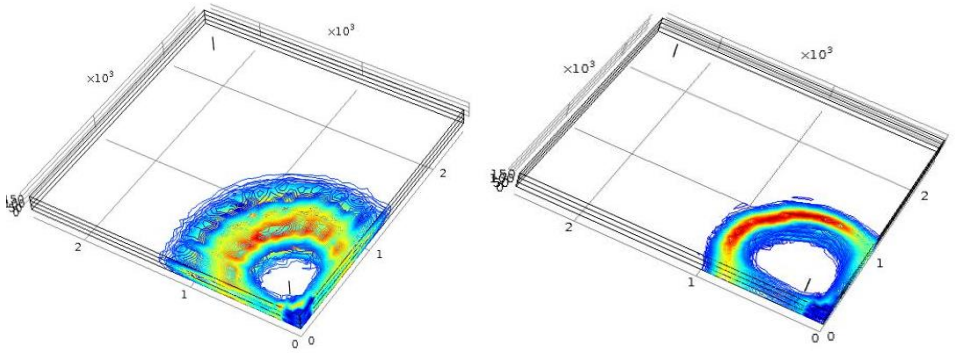

Figure 26: Heterogeneous and homogeneous anisotropic tracer's dispersion at 364th day of injection

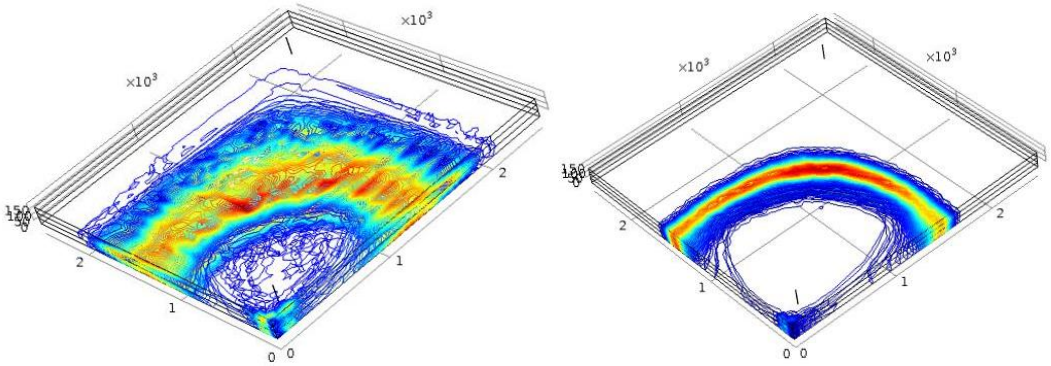

Figure 27: Heterogeneous and homogeneous anisotropic tracer's dispersion at 1001st day of injection

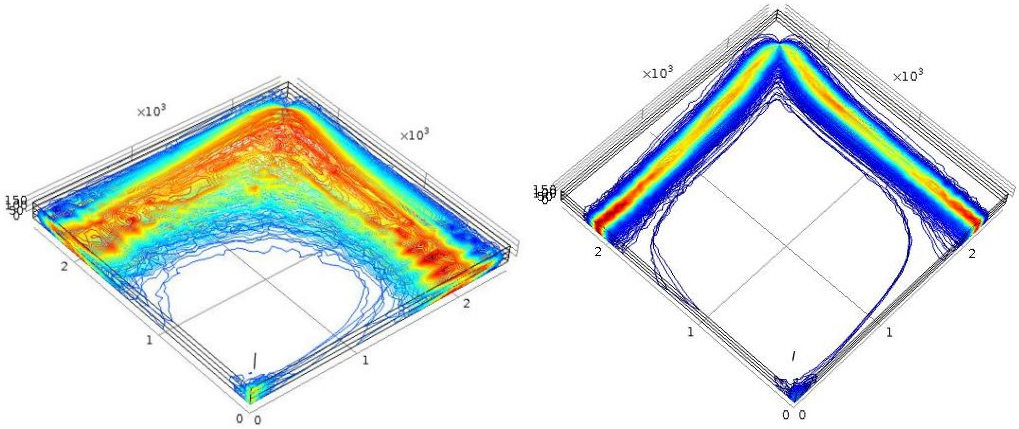

Figure 28: Heterogeneous and homogeneous anisotropic tracer's dispersion at 2506th day of injection

From the contour plots above it can be distinct that the slug moves uniformly in the porous media and the spreading is less intense in the case of the isotropic reservoir. Furthermore it is obvious that in the second case the tracer moves faster as it reaches the production well at earlier time and more quantity of the diluted is absorbed in the same period of production. This further highlights the effects of macroscale heterogeneities and anisotropy (besides pore scale velocity fields) on the hydrodynamic dispersion of diluted species. Such upscaled geological features produce preferential pathways and enhance concentration gradients, resulting in better mixing but also non-Gaussian tracer recovery curves due varying residence times of the tracer in different permeability layers.

Two more graphs will be presented at the end of this section. Normal total flux (mol/s) that is exiting the reservoir and the total quantity of mol that remains inside the reservoir during its lifetime. The two graphs are also compared with the case of homogeneous anisotropy in order for certain conclusions to be extracted.

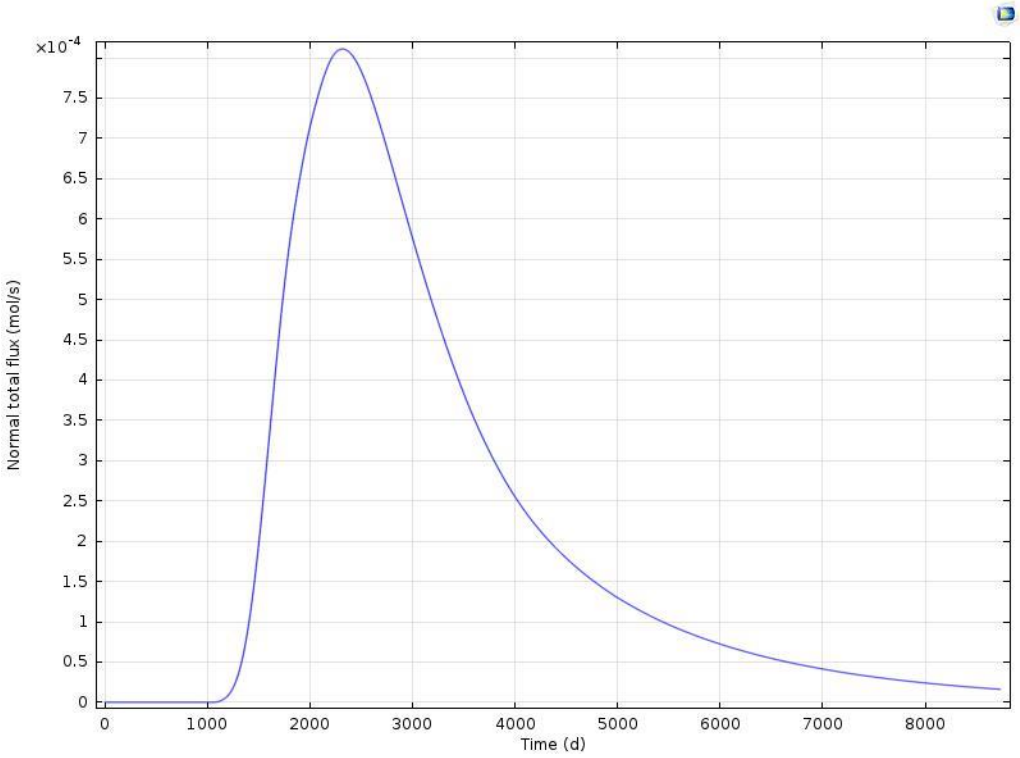

Figure 29: Normal total flux removed from reservoir during its lifetime

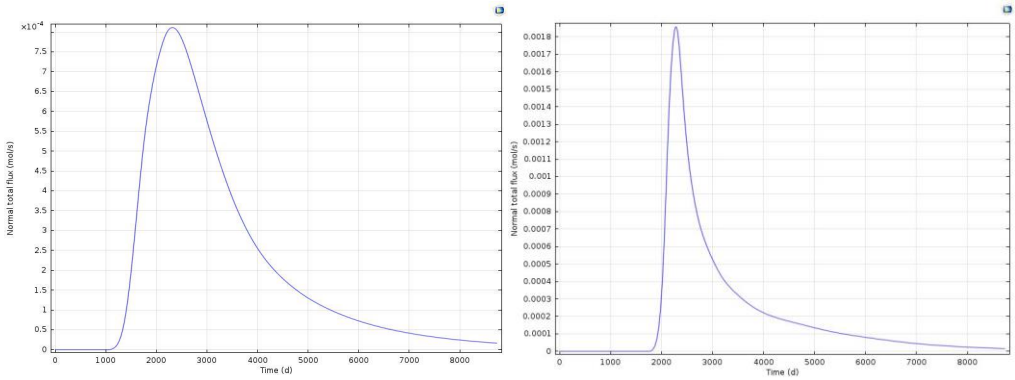

Figure 30: Comparison of normal flux removed from the reservoir between heterogeneous and homogeneous anisotropic case.

From the above graphs it can be distinct that the peak (Normal flux) that originates from the isotropic reservoir is narrower but exhibits greater quantity of mol/s at the top. It is also obvious that the tracer reaches the producer at later time (2000 days approximately). The tracer in the anisotropic reservoir reaches at 1200 days of production the production well. Moreover a more abrupt decay of the normal flux takes place earlier in the case of the isotropic geometry. To conclude, the shape of the normal flux curve can be used for the identification of the anisotropy of the reservoir in the case of lack of information about the reservoir's characteristics. The anisotropic behavior of the above peaks indicates non-Gaussian dispersion, thus a deviation from the original Gaussian dispersion behavior.

Non-Gaussian dispersion features appear when transit times through some individual heterogeneous structures become of the order of magnitude of the global transit time through the whole sample. This might be the case when very large heterogeneities with a moderate velocity contrasts with the rest of the sample are present (for instance in stratified media); this is also the case for smaller heterogeneities with a very large velocity contrast (for instance double-porosity packing of grains with a very low internal permeability acting as a dead zones). In the second case, these features are not suppressed by a flow reversal but give instead rise to both short and long time deviations from the Gaussian dispersion shapes. (Wong, 1996)

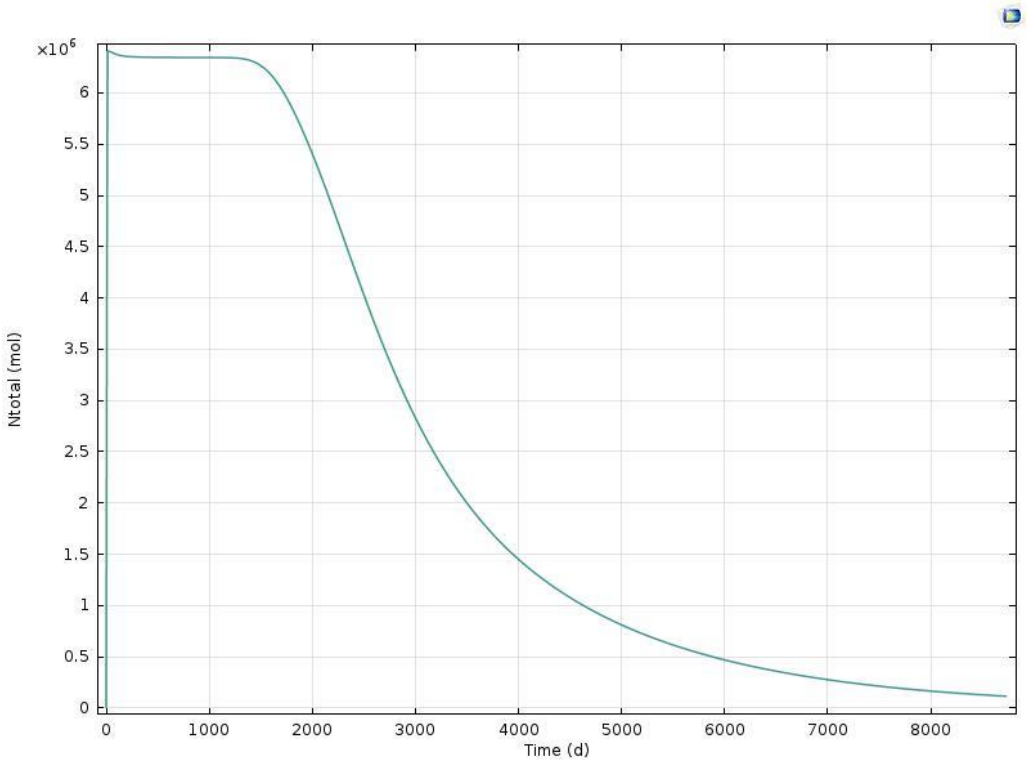

Figure 31: Total quantity of moles that exist in the reservoir while production evolves

The two graphs below present the quantity of the tracer that is left inside the system in the two cases of the isotropic and anisotropic reservoirs versus time; for the behavior of the tracer during injection and production processes to be quantified. In this comparison small differences occur between the two reservoirs. The total quantity of moles starts to decay earlier in the case of anisotropy, and that points out that the tracer reaches earlier the production well. The rate of decay of the Ntotal (moles) is similar in both cases and after 4000 days of production the quantity remaining in the system is the same.

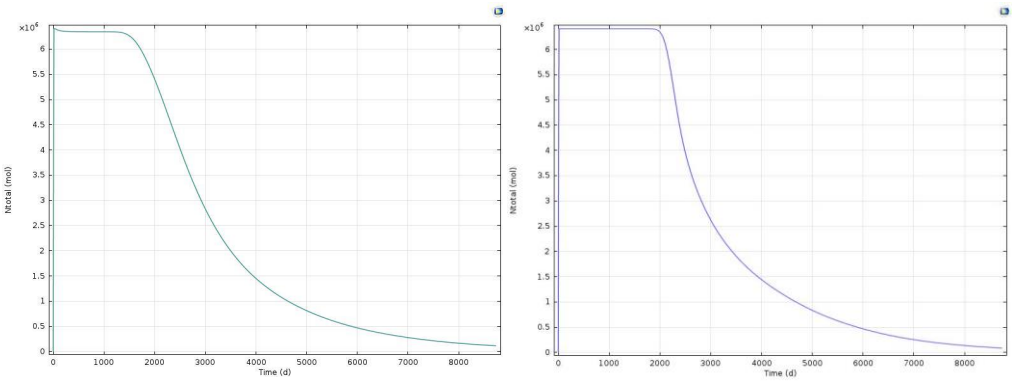

Figure 32: Comparison of the total quantity of mol that exists in the reservoir between heterogeneous and homogeneous anisotropic case.

5. Conclusion of chapter 4

In this chapter a numerical model for flow and mass transfer in a stratified petroleum reservoir is implemented using Comsol multiphysics in order to simulate hydrodynamic dispersion at the field scale. The geometry of this reservoir is stratified and consists of three anisotropic layers with different permeability. In this numerical model the dispersion coefficient is not calculated numerically, as it was in the case of the single capillary of the previous chapter, but it is introduced as an input and as a function of the local Darcy velocity. A comparison is also presented between two cases of stratified reservoirs; heterogeneous anisotropic and homogeneous anisotropic layered geometries. In an attempt to quantify the above results, the normal total flux (mol/s) that is exiting the reservoir and the total quantity of tracer mass that remains inside the reservoir during its lifetime are illustrated. The two above quantities are presented and compared in order to highlight the effects of anisotropy and heterogeneity that can be distinct and lead to non-Gaussian recovery distributions.

Chapter 5: Modeling Water - flooding in a Petroleum Reservoir

1. Introduction

Waterflooding is widely used a secondary oil recovery method. It relies on the introduction of a heavier fluid, i.e. water, in pressured depleted reservoirs in order to increase the pressure of the lighter oil phase at the production walls. In this chapter, we model two phase flow (oil and water) in the similar geometry as the one presented in the previous sections, in order to study the dynamics of secondary oil recovery. The implementation of this model is an attempt to describe two-phase immiscible incompressible flows in layered reservoir model in the presence of gravity, using Comsol multiphysics. Two phase Darcy's law interface, modified however in order to include the effect of gravity in a porous medium. The aim of this chapter is to create this model in Comsol Multiphysics and to simulate the process of water flooding. The model's geometry x, y dimensions are the same as it was in the case of the single flow of the chapter four of this thesis. The z-dimension is 50 ft instead of 150 ft and only one layer compose the reservoir's geometry. Water is the wetting phase of the reservoir and oil is the non-wetting phase. Saturation of water and pressure are two independent variables in the constitutive equations. Various types of equation system

formulations for modelling two-phase flow in porous media using the finite element method have been investigated. The system of equations consists of mass balances, partial differential equations (PDEs) that describe the accumulation, transport and injection/production of the phases in the model. In addition, several auxiliary equations (eg. hydraulic properties) apply to the system, coupling the different phases in the system together. This set of equations, PDEs and auxiliary equations, allows for equation manipulation such that the main differences between the formulations are the dependent variables that are solved for. Dependent variables of the PDE system are saturation of the wetting phase and the pressure assuming negligible capillary pressure effects at the field scale.

Firstly the pressure of the wetting phase is presented in order to identify if the model is physically correct and if there is a variance of the pressure in three dimensions due to the anisotropy of the reservoir. Then the change of saturation of the non-wetting phase due to the injection of wetting phase in the reservoir can be identified. At the end of this section a comparison is attempted with the commercial Eclipse software, which is commonly used in oil recovery studies in order to compare the quality of the results between the two models.

2. Transport equations for fractional flow theory

When two immiscible fluids with strong wettability preference are pumped simultaneously through a porous medium, they tend to flow in separate channels and maintain their identities, but with two miscible fluids no such experiment is possible. Displacement in the case of immiscible fluids is generally not complete, but a fluid can be displaced completely from the pores by another fluid that is miscible with it in all proportions; that is, in the case of miscible fluids there are no residual saturations. In the immiscible displacement process, neglecting capillarity results in the prediction of a sharp front (step function) between the displacing and the displaced phases (Buckley-Leverett profile). This situation is approached in reality when the flow rates are relatively high. At low flow rates, the effect of capillarity results in a smearing of the saturation profile. In miscible displacement there is no capillarity; instead there is mixing (Dispersion) of the two fluids. It turns out that at relatively low flow rates the effect of dispersion is slight as compared with the rate of advance of the displacing fluid. Hence, under these conditions, the approximation of using sharp displacing font is often a good one. In the case of miscible displacement the transition from pure displacing to pure displaced phase tends to become more gradual at increasing flow rates. (Dullien, 1979)

The reservoir system to be modelled consists of a five-spot pattern of four production wells surrounding each injection well. However, the symmetry of the system allows us to model a single injection production pair, which will be located at opposite corners of a grid, as shown in Figure 1. The system is initially at connate water saturation (S_{wc}), and a water flood calculation is to be performed to evaluate oil production and water breakthrough time. The reservoir will be maintained above the bubble point pressure (P_b) at all times, and thus there is no need to perform calculations for a free gas phase (in the reservoir). Reservoir and fluid properties, such as layer permeabilities, porosity, oil and water densities and viscosities and relative permeability data, are provided, as are the initial reservoir conditions and production schedule was described.

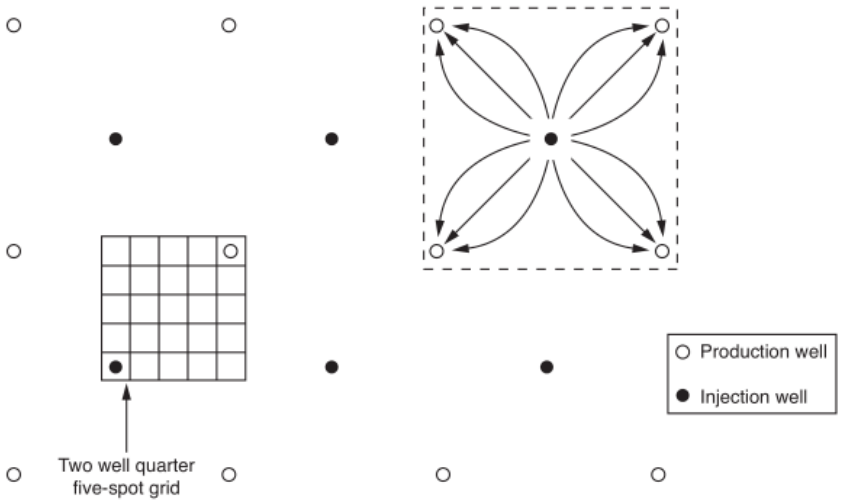

Figure 33: Five spot pattern; consisting of alternating rows of production and injection wells. (Institute of Petroleum Engineering Heriot-Watt, 2010),

The symmetry of the system means that the flow between any two wells can be modelled by placing the wells at opposite corners of a Cartesian grid. This reservoir pattern is referred to as a quarter five-spot calculation. (Institute of Petroleum Engineering Heriot-Watt 2010),

Theory of fractional flow

The fractional flow approach originated in the petroleum engineering literature, and employs the saturation of one of the phases and a global/total pressure as the dependent variables. The fractional flow approach treats the multiphase flow problem as a total fluid flow of a single mixed fluid, and then describes the individual phases as fractions of the total flow. This approach leads to two equations; the global pressure equation; and the saturation equation. (Bjørnarå and Aker, 2008)

Buckley and Leverett presented the well-known frontal advance theory. The original work was confined onto unidirectional incompressible flow through a small element of sand within continuous sand body. Along the same line of Buckley Leverett original theory, the general mass balance equation of for water phase in a multi-dimensional Waterflooding process can be written as (Xuan Zhang, 2011):

$$\phi \frac{\partial S_w}{\partial t} + \nabla * \hat{u}_w = 0 \quad \textbf{(5.1)}$$

Where S_w, ϕ, represent water saturation, porosity. u_w represent water velocity, which is a multi-dimensional vector. Total velocity of oil and water are defined as the sum of water velocity and oil velocity.

$$\bar{U} = \hat{u}_w + \hat{u}_o \qquad \textbf{(5.2)}$$

Since we assume that water and oil fill the whole porous volume, water saturation and oil saturation should result in a sum of unit and the total velocity of these two phases should obey the continuity-incompressibility equation:

$$\nabla^* \bar{U} = 0 \qquad \textbf{(5.3)}$$

According to Darcy's law, the phase velocities are proportional to the pressure gradient (which is the same in both phases due to negligible capillary forces). The proportionality coefficient for water phase, λ_w is equal to k^*kr_w / μ_w , where k and kr_w, are absolute permeability and relative water permeability, and μ_w is viscosity of water. Absolute permeabilities and, therefore, water mobility (λ_w) may be different in horizontal and vertical directions as well as at different position of reservoir. If gravity is not involved (Xuan Zhang, 2011):

$$\bar{u} = - \lambda_w \nabla p = F\bar{U} \qquad \textbf{(5.4)}$$

The velocity of oil phase is expressed in the similar way (Xuan Zhang, 2011).

$$\bar{u} = -\lambda_o \nabla p = (1-F)\bar{U} \qquad \textbf{(5.5)}$$

Where F is the fractional flow of water in the total flowing stream, defined as in terms of relative permeabilities krw, kr_o and viscosities μ_w , μ_o :

$$F = \frac{kr_w / \mu_w}{kr_w/\mu_w + kr_o/\mu_o} \qquad \textbf{(5.6)}$$

The concept of fractional flow is introduced by Leverett. When relative permeabilities kr_w , kr_o are monotonic functions of S_w , F is also monotonic function of S_w .

Substitution of expressions of velocities into flow equations leads to a closed system for water saturation S_w and pressure p .

$$\phi \frac{\partial S_w}{\partial t} + \nabla^*(-\lambda_w \nabla p) = 0 \qquad \textbf{(5.7)}$$

$$\nabla^*(-\lambda \nabla p) = 0 \qquad \textbf{(5.8)}$$

Where total mobility λ, is defined as the sum of water mobility and oil mobility:

$$\lambda = \lambda_w + \lambda_o \qquad \textbf{(5.9)}$$

Another way to express the same system in 3 Dimensions is by introducing velocities in each direction as indicated below (Xuan Zhang, 2011):

$$\hat{u}_{wx} = -\lambda_{wx}\frac{\partial P}{\partial x} \quad \textbf{(5.10.1)} \qquad \hat{u}_{nwx} = -\lambda_{nwx}\frac{\partial P}{\partial x} \quad \textbf{(5.10.4)}$$

$$\hat{u}_{wy} = -\lambda_{wy}\frac{\partial P}{\partial y} \quad \textbf{(5.10.2)} \qquad \hat{u}_{nwy} = -\lambda_{nwy}\frac{\partial P}{\partial y} \quad \textbf{(5.10.5)}$$

$$\hat{u}_{wz} = -\lambda_{wz}\left(\frac{\partial P}{\partial z} - \rho * g_g\right) \quad \textbf{(5.10.3)} \qquad \hat{u}_{nwz} = -\lambda_{nw}\left(\frac{\partial P}{\partial z} - \rho * g_g\right) \quad \textbf{(5.10.6)}$$

The system equations ***(5.1)*** and ***(5.3)*** equations presented above can be rewritten for the case of water flooding in three dimensions without the effect of gravity (Xuan Zhang, 2011) :

$$\phi\frac{\partial S_w}{\partial t} + \frac{\partial}{\partial x}\left(-\lambda_{wx}\frac{\partial p}{\partial x}\right) + \frac{\partial}{\partial y}\left(-\lambda_{wy}\frac{\partial p}{\partial y}\right) + \frac{\partial}{\partial z}\left[-\lambda_{wz}\left(\frac{\partial p}{\partial z} - \rho * g_g\right)\right] = 0 \quad \textbf{(5.11)}$$

$$\frac{\partial}{\partial x}\left(\lambda_x\frac{\partial p}{\partial x}\right) + \frac{\partial}{\partial y}\left(\lambda_y\frac{\partial p}{\partial y}\right) + \frac{\partial}{\partial z}\left[\lambda_z\left(\frac{\partial p}{\partial z} + \rho * g_g\right)\right] = 0 \quad \textbf{(5.12)}$$

The 3D water flooding system described by the two equations above aims to solve for water saturation S_w, total pressure (P) and velocities $\hat{u}_x$, $\hat{u}_y$, $\hat{u}_z$. These equations will be implemented in COMSOL to simulate the process of 3D water flooding. Also relative permeabilities (Kr_w and kr_{nw}) that are implemented inside the mobility λ_w and λ_{nw} are treated as intermediate functions dependent on water saturation S_w. (Xuan Zhang, 2011)

If fluid or matrix compressibility is considered, then appropriate compressibility coefficients also need to be defined. For the purposes of this case study all fluids, as well as the solid matrix, will be considered to be incompressible. Given this set of equations, boundary and initial conditions must be supplied to complete the mathematical description. These are usually given as known pressures, saturations or fluxes in each of the fluid phases. An important criterion for acceptance of a numerical method is that it must be able to solve the governing equations for the wide variety of possible boundary conditions. (Binning, and Celia, 1998)

Darcy's Equation for Two-phase flow

Two-phase Darcy interface uses the same equations with Darcy's but for two fluids. The implementation of the equations of the Comsol follows the fractional flow theory. A total pressure is utilized instead of two pressures, one for each wetting phase. The fractional flow theory, calculate the individual phases as fractions of the total flow. In addition, weighted averages equations are used for the description of the total density and total viscosity at each timestep. Since the saturation of each fluid is constantly changing, so is the contribution of each fluid density and each fluid viscosity. The weighted averages equations are utilized in order to simulate the compressibility of the fluids. Moreover the sum of two saturations set to be equal to unity. Finally an altered saturation equation is utilized with the use of c_1 coefficient. The two dependent variables are global pressure and c_1 coefficient, function of saturation S_1. The exact equations, this interface utilizes are presented next.

$$\frac{\partial e_p \rho}{\partial t} + \nabla * \rho \mathbf{u} = 0 \quad \textbf{(5.13)}, \; u = -\frac{k}{\mu} * \nabla p$$

$$\rho = S_1*\rho_1 + S_2*\rho_2 \textbf{ (5.14)}, \quad \frac{1}{\mu} = S_1\frac{K_{r1}}{\mu 1} + S_2\frac{K_{r2}}{\mu 2} \textbf{ (5.15)}, \quad S_1 + S_2 = 1 \textbf{ (5.16)}$$

$$\frac{\partial e_p C1}{\partial t} + \nabla*c1\mathbf{u} = \nabla*D_c\nabla c1 \textbf{ (5.17)}, \quad c_1 = S_1\rho_1 \textbf{ (5.18)}$$

The Darcy's velocity presented above, do not take into account the influence of gravity, which is a recovery mechanism really important in the description of the water flooding problem. In the model implementation part of this chapter, extra terms are added, with the use of equation view option, in order to compensate with this disadvantage of the Two phase Darcy's interface.

Description of Eclipse simulator

Eclipse is an oil and gas reservoir simulator originally developed by ECL (Exploration Consultants Limited) and currently owned, developed, marketed and maintained by SIS (formerly known as GeoQuest), a division of Schlumberger. The name Eclipse originally was an acronym for "ECL´s Implicit Program for Simulation Engineering". The Eclipse simulator suite consists of two separate simulators: Eclipse 100 specializing in black oil modeling, and Eclipse 300 specializing in compositional modeling. Eclipse 100 is a fully-implicit, three phases, three dimensional, general purpose black oil simulators with gas condensate options. Eclipse 300 is a compositional simulator with cubic equation of state, pressure dependent K-value and black oil fluid treatments.

In this Msc thesis, Eclipse 100 Simulator was utilized in order to compare the results of Comsol's two phase flow model. The equations utilized by eclipse in this specific task are presented next.

$$\frac{\partial}{\partial \mathbf{x}}\left(\frac{\mathrm{k}\mathrm{k}_{\mathrm{ro}}}{\mu_{\mathrm{o}}\,\mathrm{B}_{\mathrm{o}}}\frac{\partial \Phi_{\mathrm{o}}}{\partial \boldsymbol{\chi}}\right) + \frac{\partial}{\partial \mathrm{y}}\left(\frac{\mathrm{k}\,\mathrm{k}_{\mathrm{ro}}}{\mu_{\mathrm{o}}\,\mathrm{B}_{\mathrm{o}}}\frac{\partial \Phi_{\mathrm{o}}}{\partial \mathbf{y}}\right) + \frac{\partial}{\partial \mathbf{z}}\left(\frac{\mathrm{k}\,\mathrm{k}_{\mathrm{ro}}}{\mu_{\mathrm{o}}\,\mathrm{B}_{\mathrm{o}}}\frac{\partial \Phi_{\mathrm{o}}}{\partial \mathbf{z}}\right) = \frac{\partial}{\partial \mathrm{t}}\left(\frac{\varphi \mathrm{S}_{\mathrm{o}}}{\mathrm{B}_{\mathrm{o}}}\right) \textbf{ (5.19.1)}$$

$$\frac{\partial}{\partial \mathbf{x}}\left(\frac{\mathrm{k}\mathrm{k}_{\mathrm{rw}}}{\mu_{\mathrm{w}}\,\mathrm{B}_{\mathrm{w}}}\frac{\partial \Phi_{\mathrm{w}}}{\partial \boldsymbol{\chi}}\right) + \frac{\partial}{\partial \mathrm{y}}\left(\frac{\mathrm{k}\,\mathrm{k}_{\mathrm{rw}}}{\mu_{\mathrm{w}}\,\mathrm{B}_{\mathrm{w}}}\frac{\partial \Phi_{\mathrm{o}}}{\partial \mathbf{y}}\right) + \frac{\partial}{\partial \mathbf{z}}\left(\frac{\mathrm{k}\,\mathrm{k}_{\mathrm{rw}}}{\mu_{\mathrm{w}}\,\mathrm{B}_{\mathrm{w}}}\frac{\partial \Phi_{\mathrm{o}}}{\partial \mathbf{z}}\right) = \frac{\partial}{\partial \mathrm{t}}\left(\frac{\varphi \mathrm{S}_{\mathrm{w}}}{\mathrm{B}_{\mathrm{w}}}\right) \textbf{(5.19.2)}$$

$$S_o + S_w = 1 \textbf{ (5.20)}$$

Reservoir parameters utilized in the above equation:

Φ_o , Φ_w: Flow potentials (N*m/kg)

k: Permeability

ϕ: Porosity

S: Saturation

Kr_o , Kr_w: Relative permeability of oil and water

μ_o, μ_w: Viscocity (Pa*s) of oil and water

Bo, B_w: formation volume factor of each phase (RBBL/STB)

The equations ***(5.19.1), (5.19.2)*** presented above are solved in each grid block with the use of finite differences method.(Schlumberger 2012)

3. Model Implementation in Comsol Multiphysics

In the Chapter 5, two equations; the global pressure equation; and the saturation equation are implemented in Comsol with the use of the Two phase Darcy's law interface. The equations can be found by adding the mass balances and do some numerical manipulation for the pressure equation, and by subtracting the mass balances and some numerical manipulation for the saturation equation. Furthermore, the differential equations need to be solved together with a set of boundary conditions.

These equations are solved together as a time dependent problem for 2000 days at 1 day intervals. As Mesh settings sequence type is selected to be Physics controlled - mesh and the element size is set to be fine.

As a first step to build the model in Comsol Multiphysics the geometry of the three dimensional porous media is implemented.

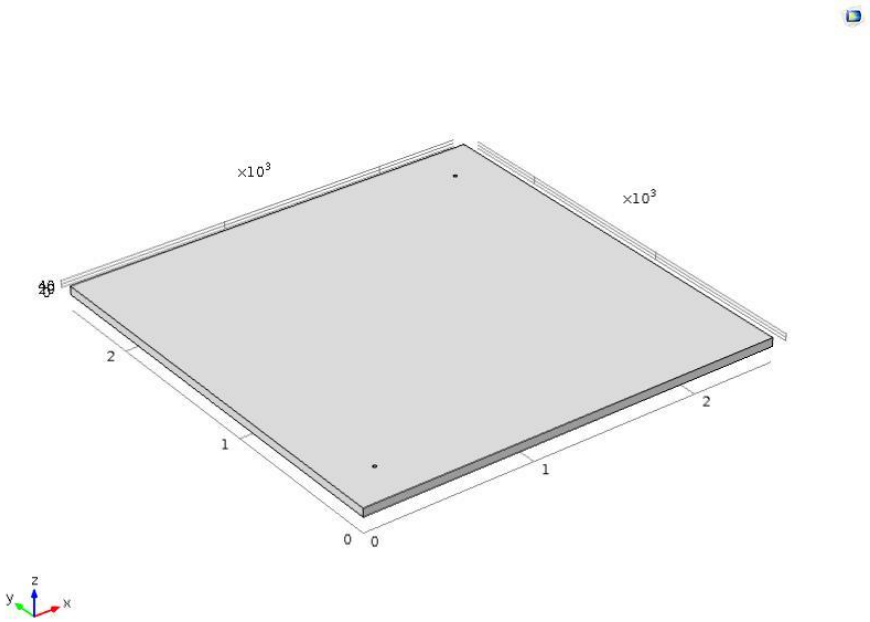

Figure 34: Geometry of the two phase flow reservoir

The reservoir geometry is similar with the one that was used in chapter four. The size of the reservoir is 2500'x2500'x50' and it consists of only one anisotropic layer. The only difference is in z-dimension's length and the total size of the reservoir is three times less than the previous case. Two wells are placed in the same location as it was in the single fluid flow case, one injection well and one production well with a radius of 10 ft each.

The mechanism than controls the secondary recovery of the reservoir is the flow of water from the injection well, and can be identified with the change of saturation of the wetting phase.

Reservoir Directions	Permeability (mD)
X	200
Y	150
Z	20

Table 3: Permeability in x, y, z directions of the two phase flow reservoir

Comsol multiphysics Two Darcy's law interface utilizes the equations of the velocities $\bar{u}_x$, $\bar{u}_y$, $\bar{u}_z$ that were described previously are a part of the Two Darcy's law interface. Furthermore porosity of the porous media, the density of the wetting and of the non-wetting phase and the initial saturations need to be selected, as it is illustrated in the table below.

Parameters	Expression – Value	Unit
Porosity	*0,2*	
Viscosity of oil	*1*	*[cP]*
Viscosity of water	*3,92*	*[cP]*
Density of water	*1000*	*[kg/m^3]*
Density of oil	*800*	*[kg/m^3]*
Capillary Diffusion	10^{-4}	$[m^2/s]$
Initial Saturation of water	*0.25*	
Initial Saturation of oil	*0.75*	

Table 4: Parameters implemented for the three dimensional; two phase flow reservoir model

Velocity components in each direction	
tpdl.ux	*(-tpdl.kappaxx*px-tpdl.kappaxy*py-tpdl.kappaxz*pz)/tpdl.mu*
tpdl.uy	*(-tpdl.kappayx*px-tpdl.kappayy*py-tpdl.kappayz*pz)/tpdl.mu*
tpdl.uz	*(-tpdl.kappazx*px-tpdl.kappazy*py-tpdl.kappazz*pz-tpdl.kappazz*tpdl.rho*g_const)/tpdl.mu*

Table 5: Gravity effect added in the third component of velocity; with the use of the two Darcy's interface of Comsol Multiphysics.

Relative permeabilities of the wetting and non-wetting phases were introduced as function of water saturation. The graphs below indicate the Kr_w and Kr_{nw} relationship with S_w.

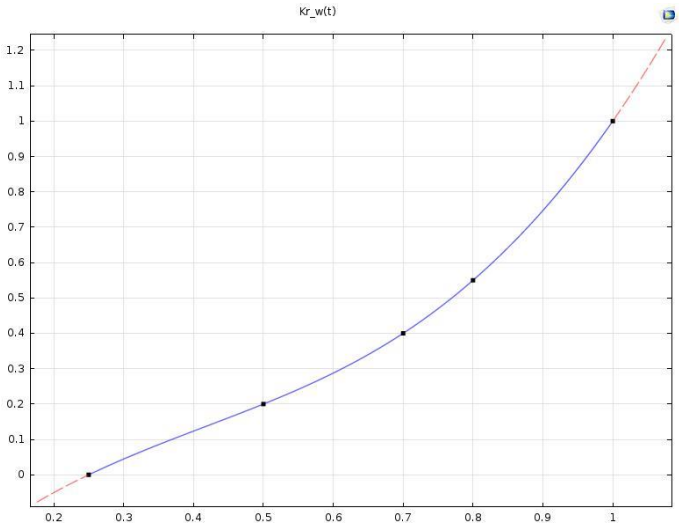

Figure 35: Relative permeability of water (Kr_w) as a function of water saturation

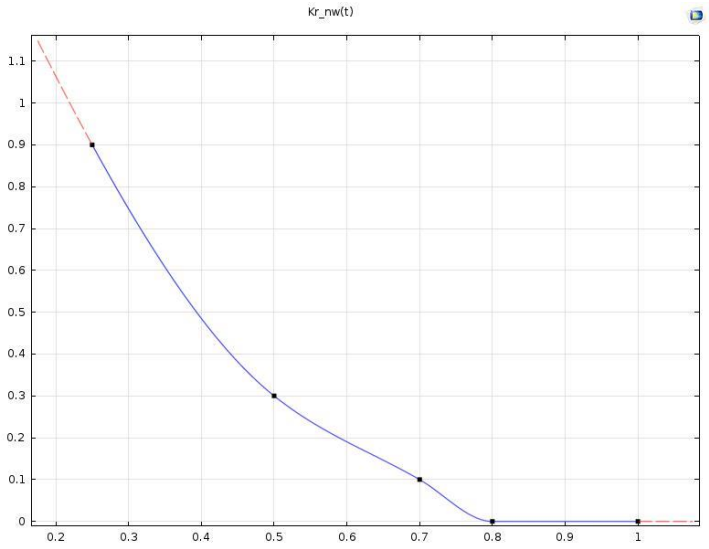

Figure 36: Relative permeability of oil (Kr_{nw}) as a function of water saturation

Interpolation functions were implemented in Comsol's Model in order for the above graphs to be used in the calculations of the water flooding simulation. Relative permeability of the water was introduced in Two Darcy's interface as kr_w(tpdl.s1) and relative permeability of the oil as kr_nw(tpdl.s1).

Boundary conditions

As a next step of the procedure, tpdl.rho1*g_const*(2453.64-z)+10^5 Pa initial value for pressure regime is defined together with initial saturation of 0.25. The same value is set for the production well outlet and this value will be the controlling parameter of reservoir's production. No flux boundaries (-n*ρu = 0) are set in every wall of the reservoir at the side and at the top and the bottom of the model's geometry. Finally the normal inflow velocity of the injection well is set constant at 6.983*10^{-5} m/s and the saturation of the fluid is also set to unity.

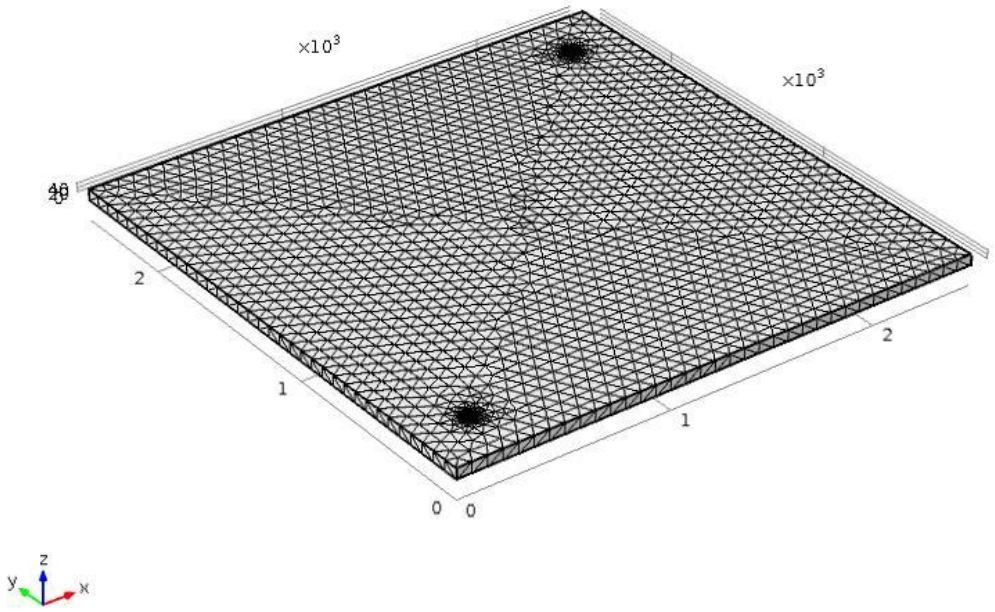

Figure 37: Fine element size – Mesh selected in 3D Geometry model.

The above mesh sequence physics control option was selected and the size of the element was selected to be fine. It can be distinct that in the area around the wells the element size is even finer in order for the simulation to be more detailed in those areas.

4. Results & Discussion

In Figures 38-40, we present the streamlines and wetting phase velocity arrows. As expected, the flow of the wetting phase is from the inlet to the production well, with higher velocities observed closer to the wells where there is limited space for flow. Accordingly the pressure profiles of figures 44 - 47, show the dynamics of water pressure with higher pressures closer to the injection well and closer to the bottom of the reservoir due to hydrostatic pressure. Furthermore, saturations of the wetting and non-wetting phase are presented in order to identify the impact of the secondary recovery process in the production of oil. Moreover, Stock Tank Barrels/day of oil that are produced, and bottom hole pressure (Pa) of injection and production well are presented. Finally a comparison with the results of the Eclipse simulator is attempted, in order to evaluate Comsol's multiphysics model.

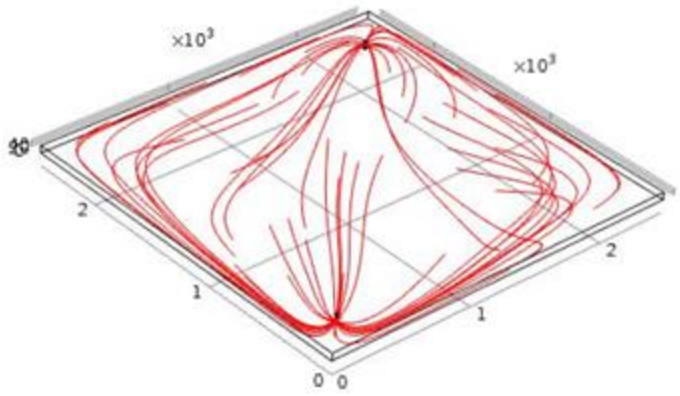

Figure 38: Streamlines in two phase flow simulation; representing velocity field

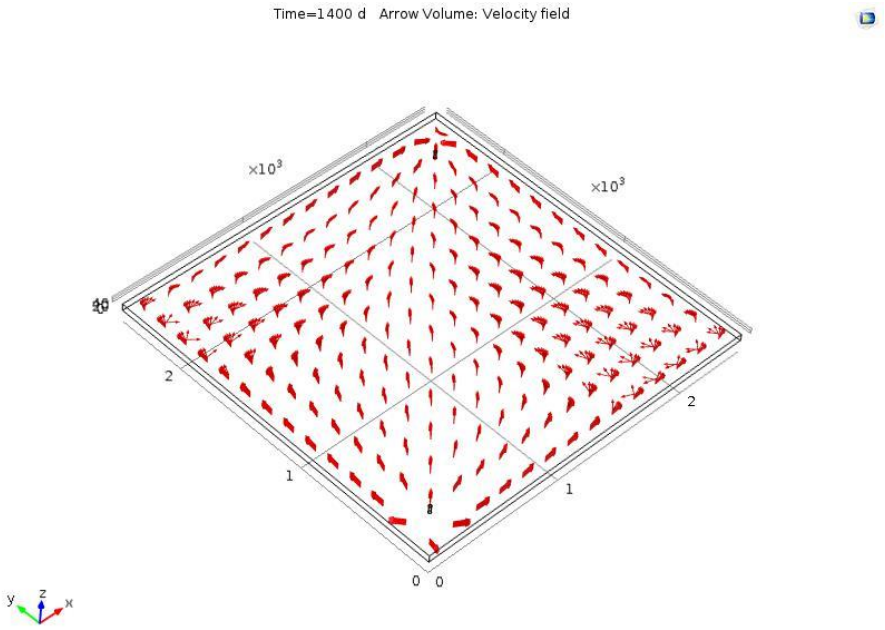

Figure 39: Streamlines in two phase flow simulation; representing velocity field

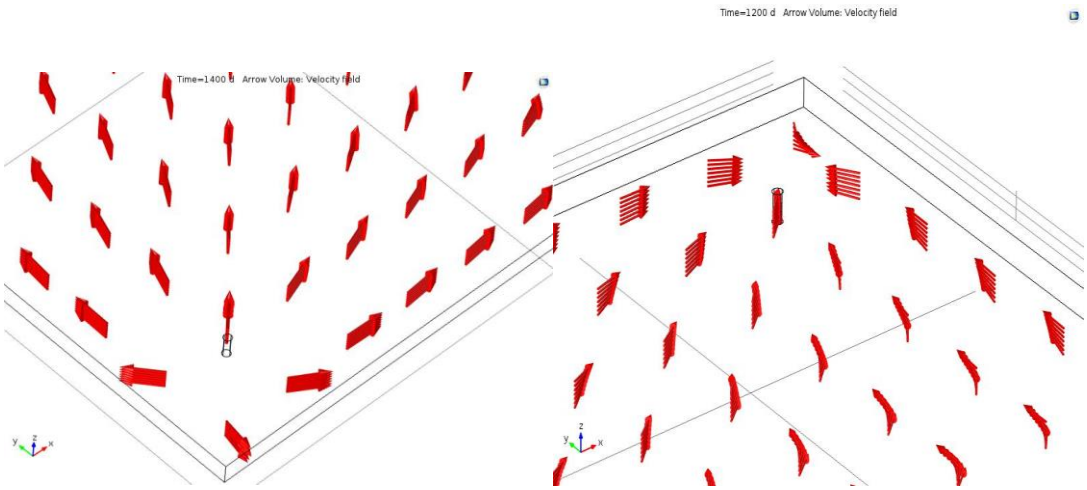

Figure 40: Arrows indicating velocity field in the two wells; left part injection well & right part production well

In figures 41, 42 the pressure regime is illustrated with the use of contour plot, at various times, in order to point out the transient change of pressure due to injection of water throughout the Waterflooding process. The greater impact in the change of pressure can be identified up to 800 days on water injection, after that the pressure change cannot easily be distinct. Before comment on this fact, it is useful to understand the representation of the saturation pointed out in figure 43. In this figure the displacement of the oil is obvious as the injection of the water procced. Contour plots are also used, illustrating the extent of the saturation of the wetting phase rise, in the reservoir. After 600 days of injection the greater part of the reservoir is saturated with the injected water, meaning that a significant quantity of oil is produced. The change of saturation of the wetting phase due to the non-wetting phase displacement leads to the change of pressure regime that is illustrated in figures 41, 42.

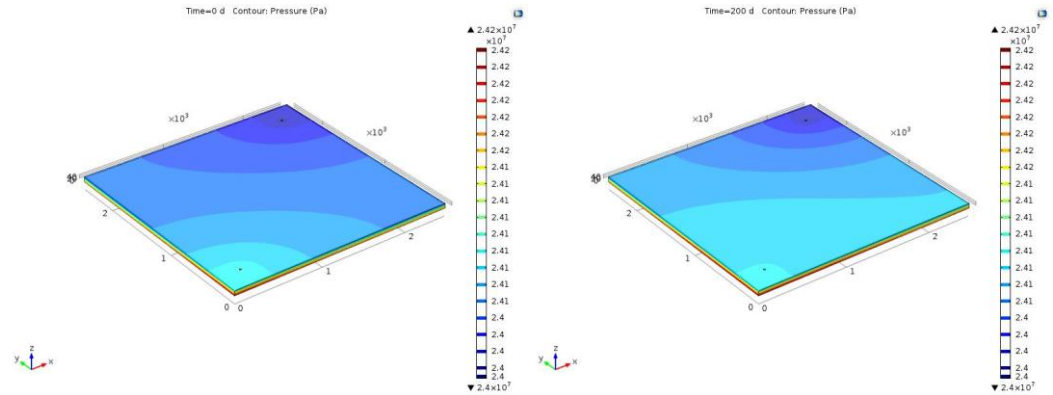

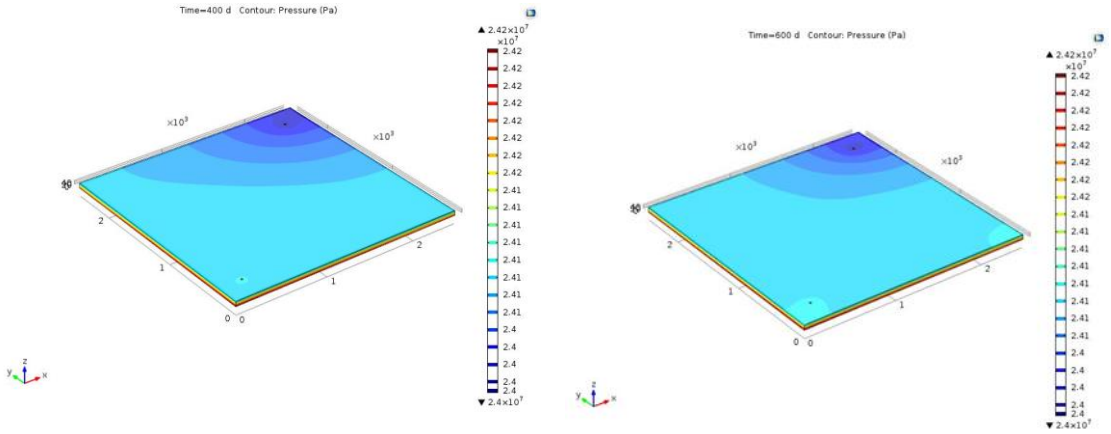

Figure 41: Pressure regime in two phase flow simulation at 0 to 600 days of injection

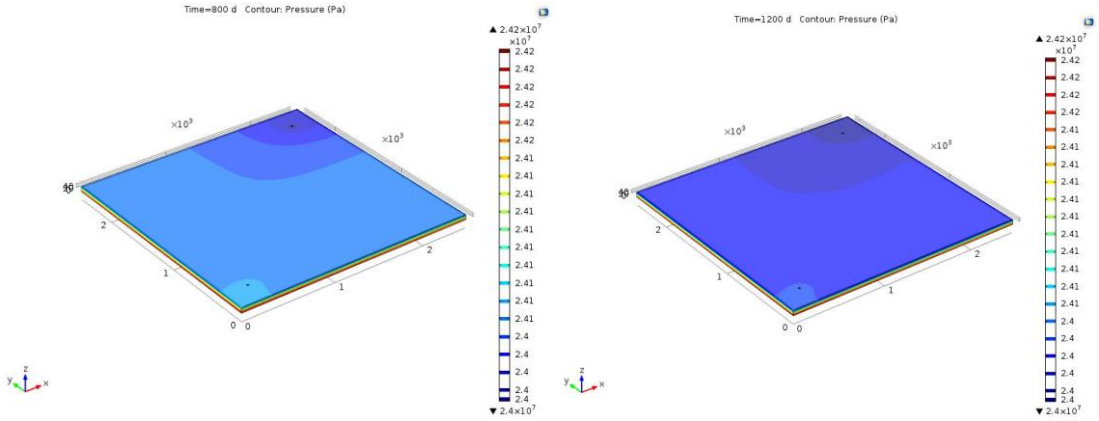

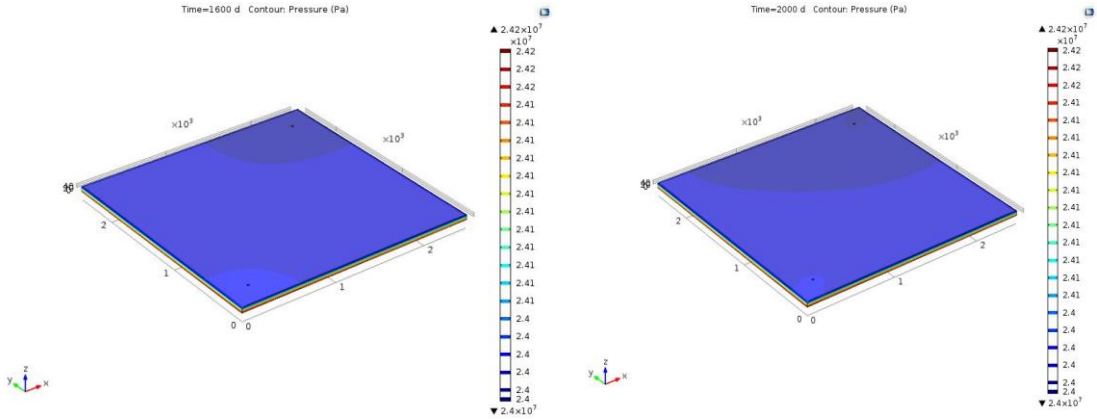

Figure 42: Pressure regime in the two phase simulation at 800 to 2000 days of injection

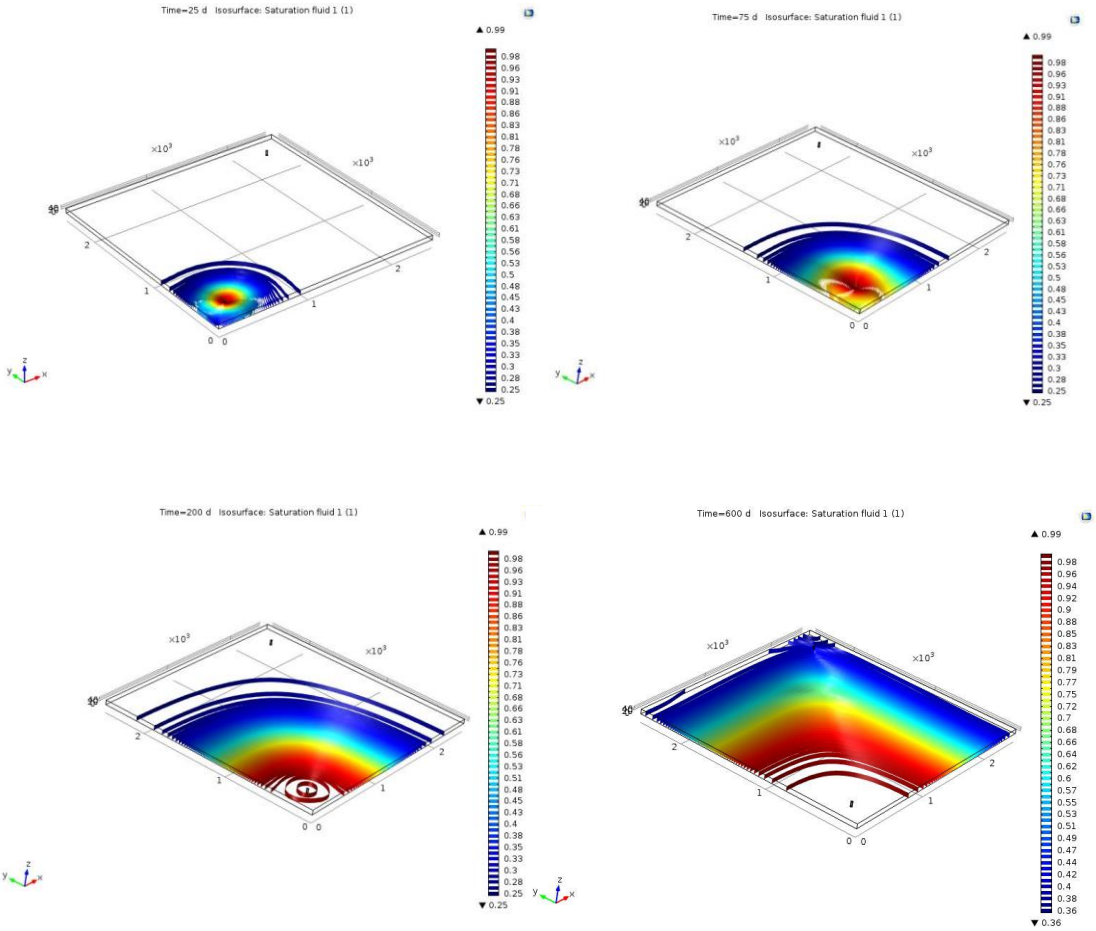

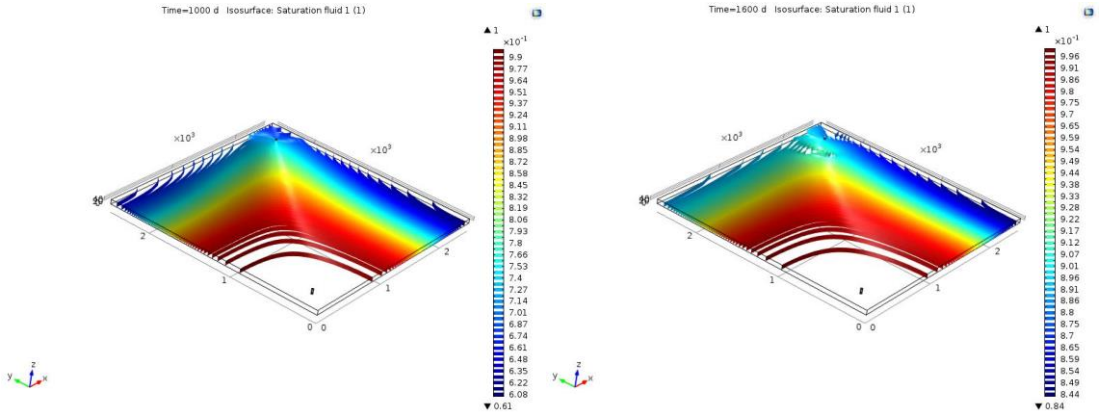

Figure 43: Representation of Saturation evolution of the wetting phase in in 25th, 75th, 200th, 600th, 1000th and 1600th days of injection.

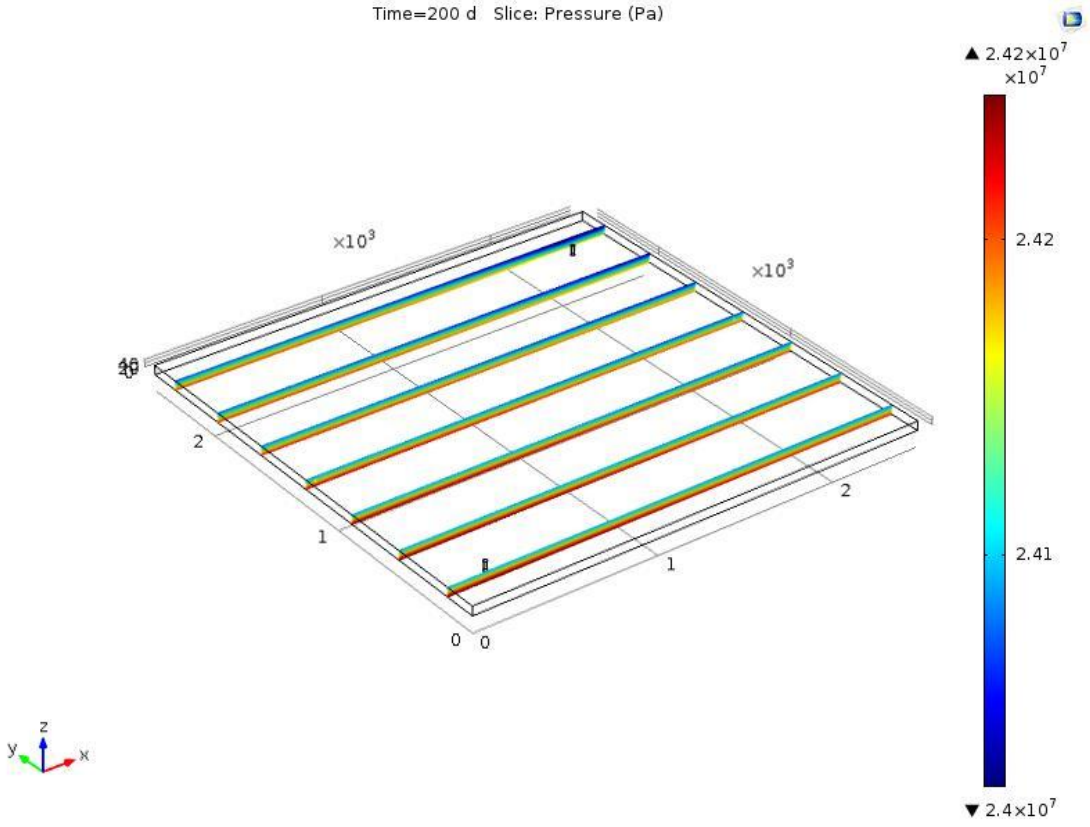

Figure 44: Pressure variation in z direction; 200th day of injection

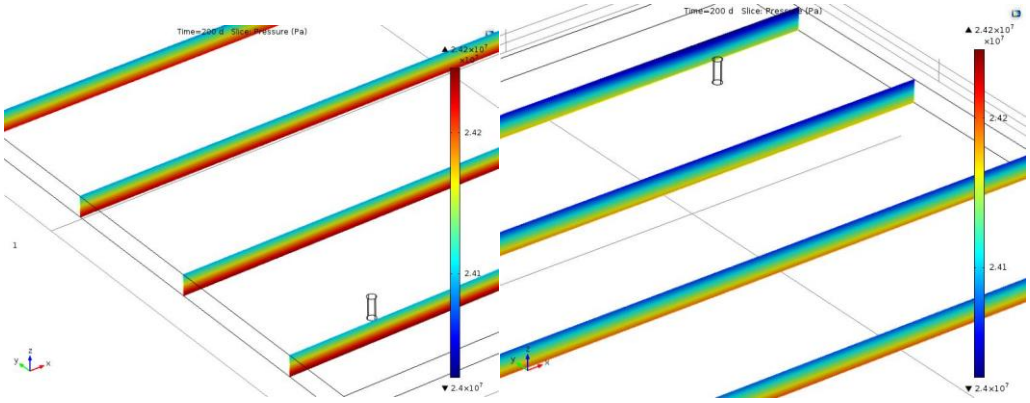

Figure 45: Pressure variation at injection (left) & production (right) well; 200th day of injection

In figures 44-48 the effect of gravity that leads to pressure variation in z direction can be identified. The figures illustrate the pressure regime that is enforced in the reservoir and points out the difference degree of change in pressure between the injection and the production well at two different times. Figures 44 and 45 present pressure at 200th day of water-flooding in the reservoir, and at the near area of both wells. It can be distinct that the pressure variation is really different in the production well, due to the fact that at this period of production the area around the well has a significant quantity of oil instead of water; that is around the injection well. Figures 46 and 47 present the pressure change due to gravity in the same areas as before, but at 1000th time of production. In those figures the pressure change is different if the production well is compared with the previous time. This is due to the fact that water flooding has proceeded to a greater extent and has reached the area around the production well; changing this way the pressure regime.

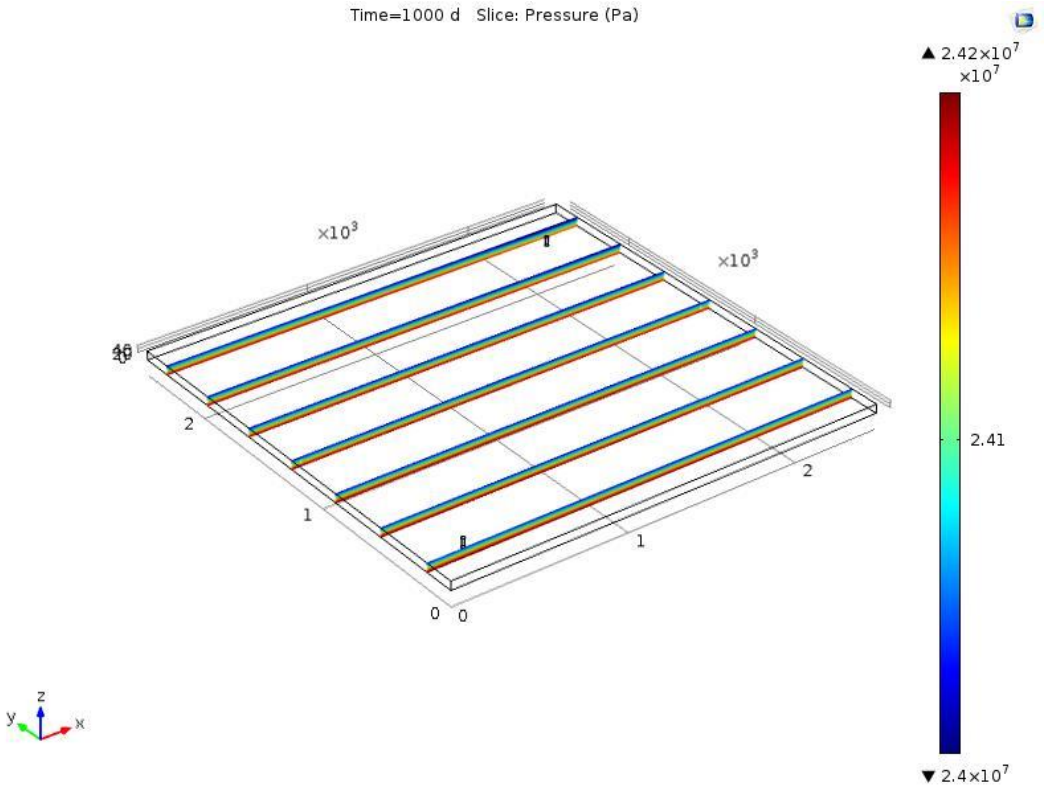

Figure 46: Pressure variation in z direction; 1000th day of injection

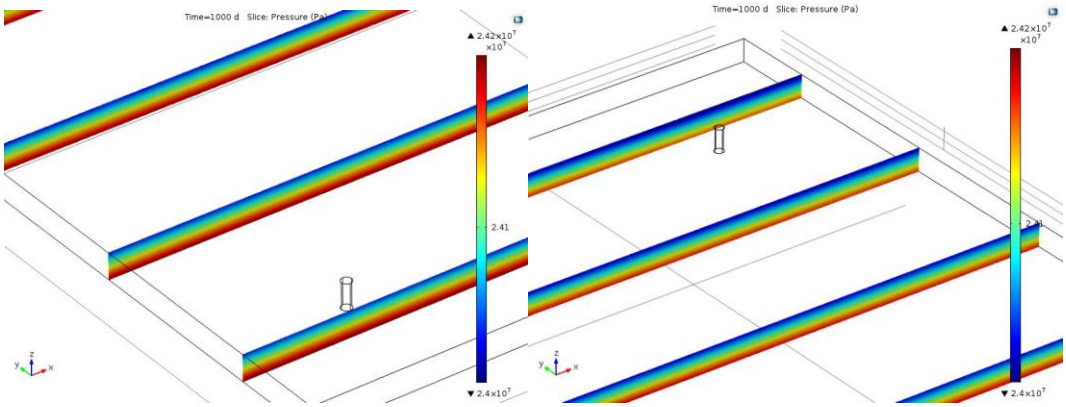

Figure 47: Pressure variation at injection (left) & production (right) well; 1000th day of injection

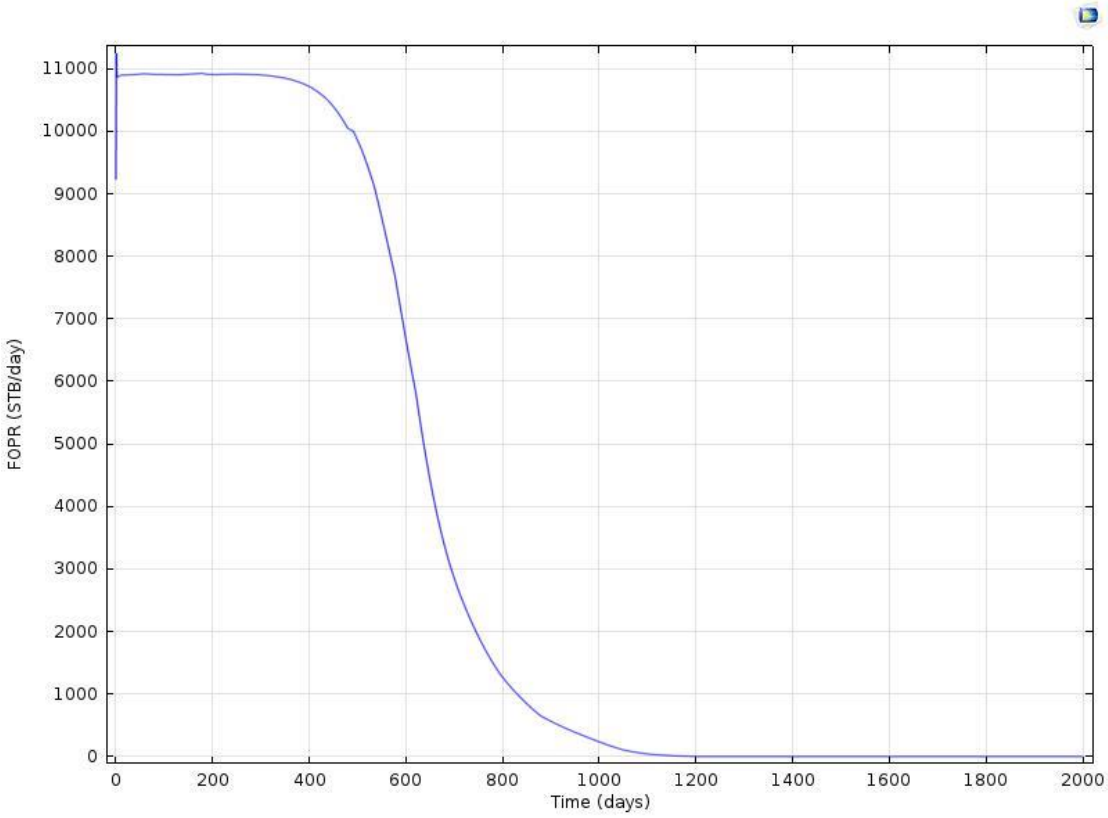

Figure 48: Stock Tank Barrels/day of oil produced, throughout secondary recovery process

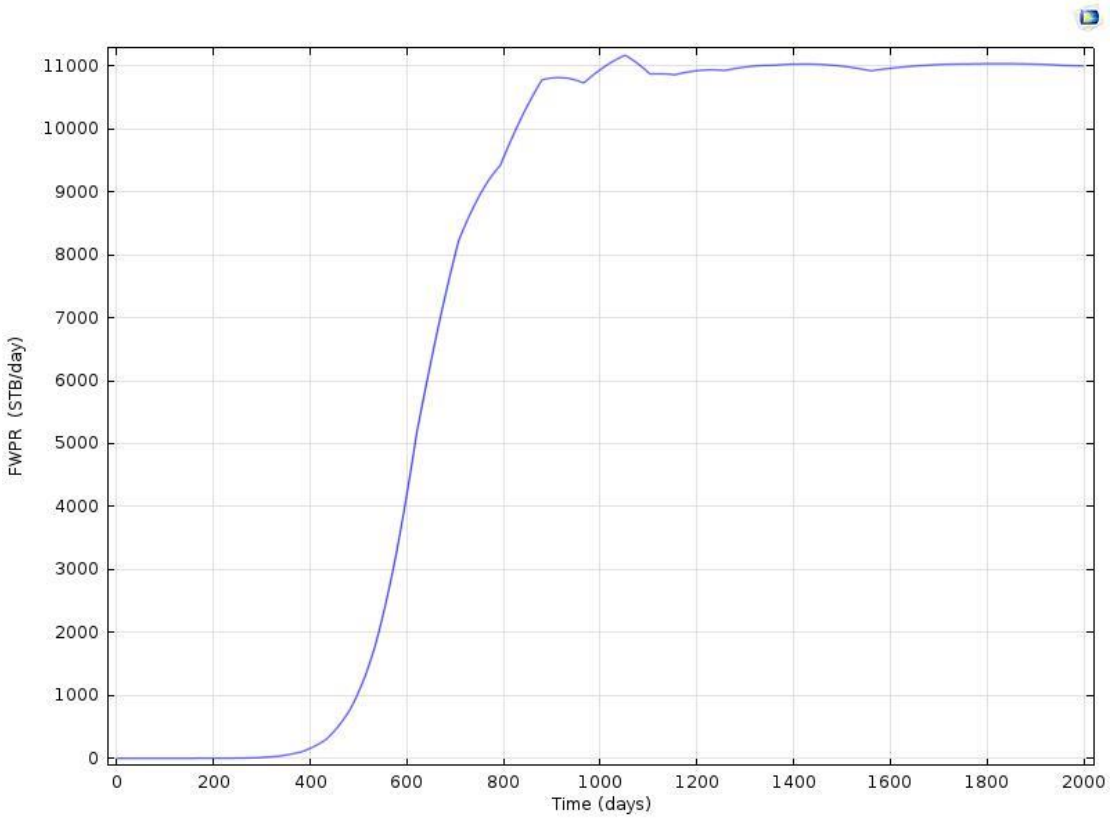

Figure 49: Stock Tank Barrels/day of water produced, throughout secondary recovery process

In Figure 48 the Stock Tank Barrels/day of oil that are produced at water-flooding process. After a few days the production rate reaches a plateau, at about 3400 STB/day, until 600 days of injection. From this time and on, the production rate starts decaying smoothly until the end of reservoir's life; after 2000 days of production. Since the bottom hole pressure is set constant in order to control the production of oil, the production rate reaches a plateau until a point where the bottom hole pressure cannot sustain this production rate.

In figure 49 the Stock Tank Barrels/day of water that are produced at water injection process are presented. Water production is zero at the start of production; since the initial saturation of 0.25 indicates the irreducible quantity of water, which is immobile. After 600 days of production the water production starts rising due to the fact that the injected water has reached the area around the production well. From this point and on, the quantity of water produced continue rising until the end of reservoir's production.

In figures 50 and 51 bottom hole pressure of injection well and the average reservoir pressure are presented throughout the secondary recovery process. The pressure of the production well is set constant at $2.407 * 10^7$ Pa. The injection well bottom hole pressure is increasing and reaches a maximum after approximately 600 days of production. This effect has to do with the increasing quantity of water that is introduced in the reservoir. Since a quantity of oil is removed at the same time that water is injected in the system, after some point due to the quantity of fluids that are removed the pressure starts decaying. The decay of the pressure appears after approximately 600 days until the end of reservoir's production

at the 2000th day. The average reservoir pressure starts rising from a value of 2.413 * 10^7 Pa. Pressure of the system, due to water injection, is increasing and reaches a peak at 600 days of production. From this point and on, the average reservoir pressure starts to decline until the end of reservoir's life, due to the change in average viscosity of the reservoir.

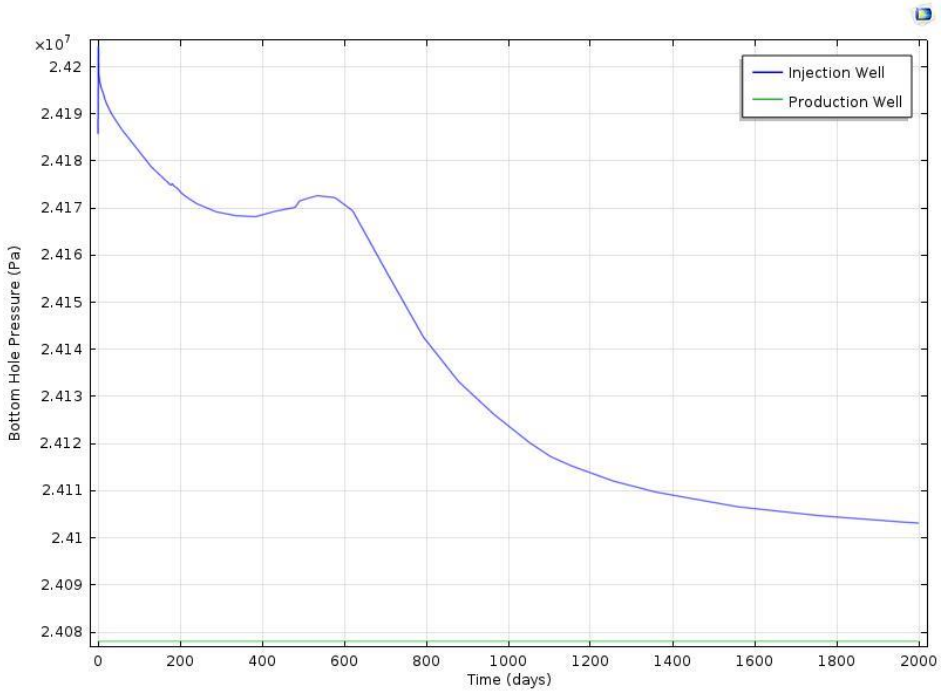

Figure 50: Bottom Hole Pressure of injection & production well throughout waterflood process

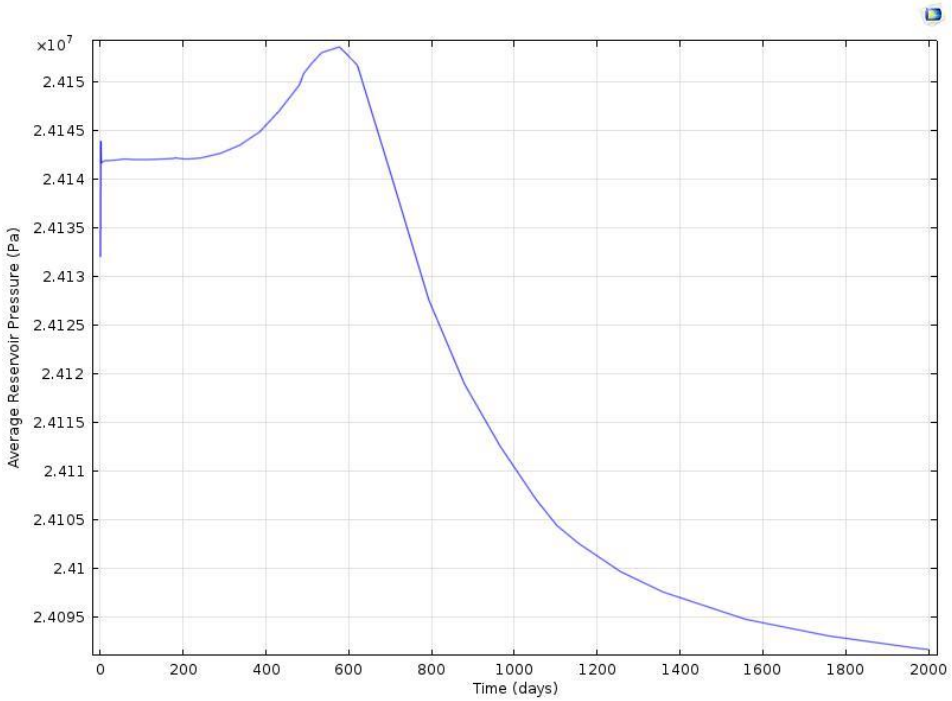

Figure 51: Average Reservoir Pressure throughout waterflood process

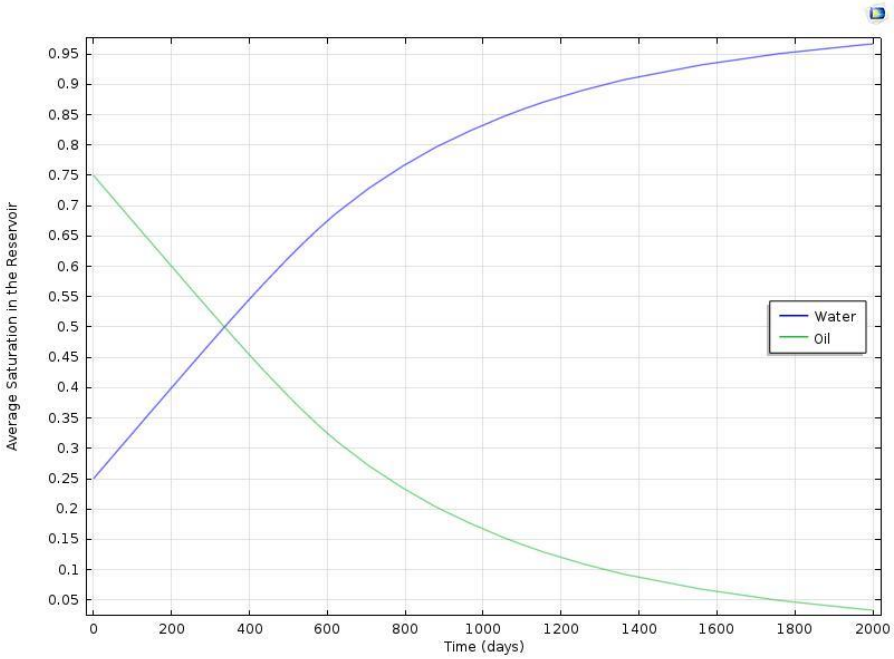

Figure 52: Average Saturations of Water and Oil, throughout waterflood process

Figure 52 is presented in order to point out the change in average saturation of the wetting and the non-wetting phase of the reservoir, from the beginning up to the end of water injection process. The trends that are illustrated in the above figure ensure that the numerical model is physically correct since the average saturations of the two phases are inversely proportional. At the end of the Waterflooding the reservoir is fully saturated with water, since the greater part of oil is produced

Comparison with Eclipse simulator

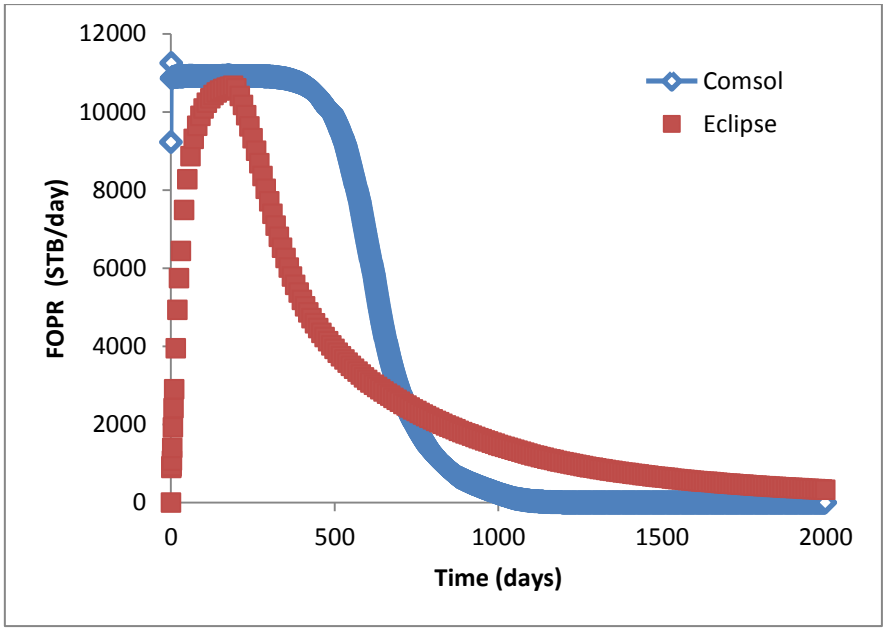

Figure 53: Comparison of Stock Tank Barrels/day of oil produced with the two simulators

In figure 53 the oil production rate with the use of both simulators is compared. Both simulators predict a maximum production rate of 11000 STB/day but it can be distinct that Comsol overpredicts the period that maximum production rate holds during Waterflooding process in comparison with eclipse simulator. Moreover, for eclipse simulator's results the change of rate from the maximum to lower is more abrupt, a behavior that usually holds true is similar reservoir production cases. Finally the oil is extracted from the reservoir, in Comsol model, after 1000 days of production. In the case of Eclipse simulation, oil is recovered from the reservoir at approximately 1700 days of Waterflooding. Differences that were aforementioned and the fact that oil production, in Comsol model, do not initiate from zero and then increase gradually, as in the case of eclipse simulator, point out that certain numerical instabilities have encountered in the model.

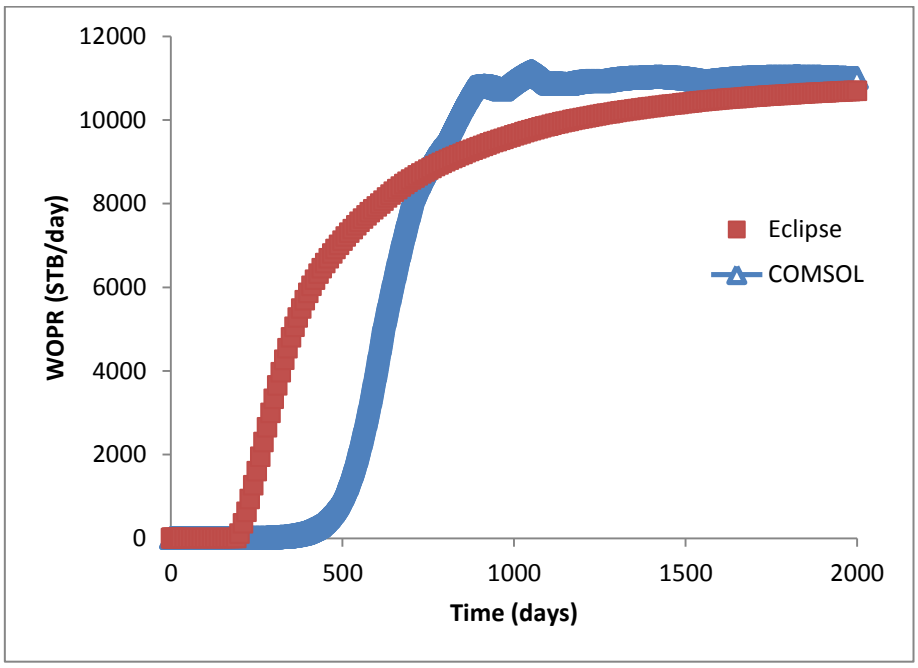

Figure 54: Comparison of Stock Tank Barrels/day of water produced with the two simulators

In the above figure, water production rate for both simulators is presented and compared. Since the initial quantity of water in the reservoir is immobile, the first traces of water identified in the producer reveal the water breakthrough. In the model implemented in Comsol, water breakthrough takes place at approximately 450 days of Waterflooding counter to 250 days of production in the case of eclipse simulator. As soon as tracer quantities of water appear in the production well, production of water rises gradually in both simulators. After 1000 days of production two peaks point out the numerical instabilities that were identified also in the figure 53. Finally with a different rate both simulators reach a plateau at 11000 STB/day; steady state is achieved as soon as oil quantity is removed from the reservoir. This figure indicates that as far as the production of water is concern, Comsol model and Eclipse simulator provide an adequate matching in the behavior of the reservoir.

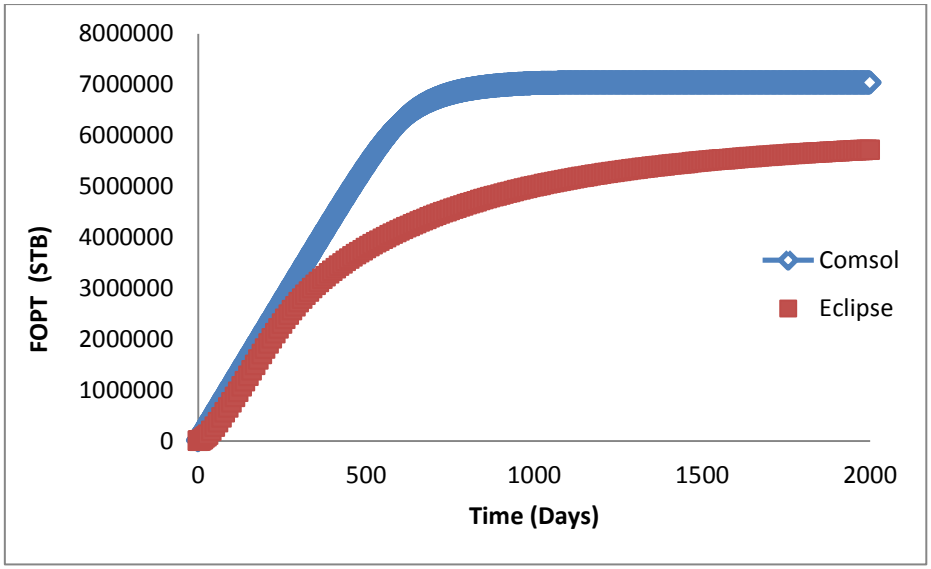

Figure 55: Comparison of cumulative oil (STB) produced with the two simulators, throughout Waterflood process

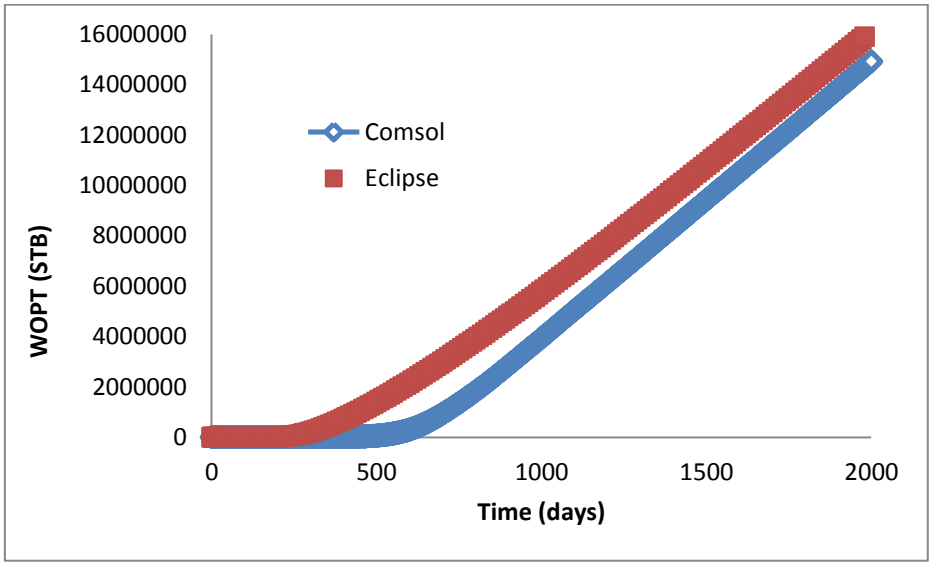

Figure 56: Comparison of cumulative water (STB) produced with the two simulators, throughout Waterflood process

The behavior described in figures 53, 54 is illustrated with a different way in figures 55, 56. Cumulative quantities of oil and water that are produced throughout waterflood process are presented and compared. The integral of the rate of production of each fluid is described by the cumulative quantity of each phase. Figure 55 reveals that Comsol model overpredicts the quantity of oil produced in comparison with Eclipse simulator, after the water breakthrough. Figure 56 points out that Comsol's model under predicts the production of water, but deviation is in a smaller extent than in the case of oil production.

Numerical instabilities are identified from the comparison of the two simulators of reservoir's behavior throughout Waterflooding process. The main reasons for those differences are the deviation in the drainage areas of the two models and the difference in the implementation of relative permeabilities in both simulators. The model implemented in

Comsol multiphysics describes the production and the injection wells as cylinders with a radius of 10 ft and a height of 50 ft. The boundaries of each cylinder, is selected as the inlet and the outlet of the reservoir's water injection process. The inflow of 11000 STB/days of water injected, is introduced as an inlet velocity and is adjusted to the area of the cylinder in order to have identical conditions with the injection well of the model that eclipse simulator utilizes; Eclipse uses in both wells a point source for production and injection wells. In the case of production well the outlet conditions applied, and thus the controlling mechanism of production is a constant pressure. Due to the fact that the production is controlled by a constant value of pressure, the rate of production cannot be controlled and that results to an area around the production well with deviations between the two models. In figures 35 & 36 the relative permeabilities kr_w and kr_{nw}, as functions of water saturation, of the two phases that were introduced in Comsol's model are presented. In addition equation ***(5.12)*** describes the way that relative permeability is introduced in Comsol's numerical model, through average viscosity of the total fluid which is changing as the saturation of water is rising. On the other hand, equations ***(5.19.1)*** and ***(5.19.2)*** describe the way that relative permeabilities are introduced in the three dimensions of the reservoir in eclipse simulator. It is obvious from the results extracted that numerical instabilities can be identified also at the initial and at the final values of saturations at the edges of relative permeabilities functions. This behavior leads to the conclusion that the extrapolation out of the relative permeabilities range is unstable.

The equations (PDEs) that are utilized in Comsol multiphysics are a realization of fractional flow theory. Fractional flow treats the multiphase flow problem as a total fluid flow of a single mixed fluid, and then describes the individual phases as fractions of the total flow. This approach and the fact that Comsol cannot identify the immobile quantities of each phase, since it address the two phase flow as a single phase flow simulation problem, leads to uncertainties about the quality of the results extracted. On the contrary, spatial resolution (Mesh instead of grid) and time stepping are finer in Comsol multiphysics and thus there is a more detailed description of the solution. Nevertheless, as a result of the geometry of the problem the grid orientation effect arises when Eclipse simulator is utilized. This phenomenon is particularly severe in reservoir simulation and in certain cases it can increase substantially the uncertainty of the numerical predictions. In the grid geometry that is used in eclipse simulator, there is fluid flow oriented with diagonally across the grid. If the two wells were oriented with the principal grid direction the results of the simulation would be different. This can produce simulations for two phase flows with unphysical results. In Comsol multiphysics the use of triangular mesh and the fact that the problem is solved continuously; the orientation effect is avoided.

Moreover Comsol software is equipped with a graphical interface to use when the numerical model is implemented. The PDES that are solved to describe the physical problem can be identified and the user can interfere and implement a change if it is a necessity for the problem. In the case of the two phase flow problem, the Two-Darcy's interface did not include the effect of gravity. In order for the numerical model to be consistent with the physical reality of Waterflooding process, additional terms were added in the PDEs that Comsol utilizes. Eclipse simulator uses finite differences method to solve the PDEs of the problem and Taylor's expansion for the approximation of the derivatives. Comsol

Multiphysics uses finite elements method; reduces the number of unknowns and thus the complexity of the simulation. To conclude, eclipse utilizes more precise description of the reservoir simulation problem, since it uses different equation for each phase and Comsol utilizes a single equation and time dependent average quantities of density (ρ) and viscosity (μ) and the saturation of the wetting phase, as a dependent variable. The way that the PDEs are solved in time and in space is more detailed in Comsol multiphysics and cost less in computation time; advantage in comparison with Eclipse reservoir simulation software.

5. Conclusion of chapter 5

A numerical model for two-phase flow under gravity was implemented in Comsol Multiphysics in order to simulate process of water flooding during secondary oil recovery in heterogeneous and anisotropic three dimensional reservoirs. In the above model relative permeabilities of the wetting and non-wetting phase were introduced as functions of water saturation (S_w). The purpose of this study is to obtain information about the production rate in STB/day of oil and water that are produced during the entire lifetime of the reservoir. The effects of gravity on pressure dynamics are then illustrated in two different times for the reservoir and in the area around the two wells, as the oil saturation changes locally towards smaller values. The calculated values of bottom hole pressure for the injection well indicates that pressure is increasing up to a maximum value and then starts decreasing until water breakthrough takes place at the production well of the reservoir. At the end of this chapter the results obtained from Comsol's numerical model are compared with those of the Eclipse simulator for the same reservoir simulation problem. The general response of the reservoir is described adequately from both simulators, in terms of both oil recovery rates and cumulative recovery. While in general good agreement, the numerical predictions of the two models also exhibit distinct differences that should be attributed to the numerical scheme used to solve the PDE's and the effects of discretization, rather than the underlying physical model, which is essentially the same in both cases. This particular point however deserves further investigation in a future study.

Conclusions of Msc thesis

Three numerical models were implemented in Comsol multiphysics in order to model single and multi-phase flows in petroleum reservoirs. Firstly the effect of hydrodynamic dispersion arising in the pore scale is reproduced. The influence of the parabolic pore scale velocity profile in hydrodynamic dispersion coefficient in contrast to the flat velocity profile is identified. Next hydrodynamic dispersion at a three dimensional reservoir is modeled, in an attempted to point out pore to field-scale impact. Heterogeneous anisotropic and homogeneous anisotropic layered reservoirs geometries are under the scope of this thesis, and a comparison between non-Gaussian recovery distributions is illustrated in figures 30 & 32. In the last numerical model two-phase flow under the presence of gravity, simulate the secondary recovery process of water-flooding in a homogeneous anisotropic reservoir. Results of the change in pressure regime and in saturation are presented in figures 41, 42 & 43. As a last step, a comparison with the results of Eclipse reservoir simulator (53-56 figures)

is attempted to evaluate the possibility of whether Comsol Multiphysics can reproduce the oil & water production rates provided by the widely used software of the oil industry. Comsol Multiphysics 5.0 simulate successfully all three numerical models pointing out that pore scale effects such as hydrodynamic dispersion determine the field scale transport properties. A comparison of the two reservoir simulation models present acceptable matching; indicating that Comsol multiphysics can be used as a reservoir simulation alternative for the oil industry.

As a recommendation for future work, simulation of Waterflooding process in a stratified geometry could be implemented in Comsol multiphysics and a comparison could again be attempted with Eclipse simulator of Schlumberger, for the same reservoir simulation problem.

References

Bear, J. (1972) *Dynamics of fluids in Porous Media.* New York: Dover Publications

Bear, J. (1979) *Hydraulics of Groundwater*, New York: McGraw-Hill

Bear, J., & Bachmat, Y. (1967) A generalized theory on hydrodynamic dispersion, Proc. I.A.S.H. Symposium on Artificial Recharge and Management of Aquifers, IASH Publ.

Binning, P. & Celia, M.A. (1998) Practical implementation of the fractional flow approach to multi-phase flow simulation. Advances in Water Resources Vol. 22, No. 5

Bjørnarå, T. I. & Aker, E. (2008) Comparing Equations for Two-Phase Fluid Flow in Porous Media, COMSOL Conference 2008 Hannover

COMSOL (2013).COMSOL Multiphysics, 4.3b Reference Manual. Version COMSOL 4.3b .

COMSOL (2013).COMSOL Multiphysics, 4.3b Subsurface Flow Module User's Guide. Version COMSOL 4.3b .

COMSOL Multiphysics 2015. PDE equations. Available from: <http://www.comsol.com/multiphysics/navier-stokes-equations>.[10 july 2015]

COMSOL Multiphysics 2015.Longitudinal and Transverse dispersivity.Available from: <https://www.comsol.eu/model/effective-diffusivity-in-porous-materials-978>.[30 july 2015]

Dullien, F.A.L. (1979) Porous Media: Fluid Transport and Pore Structure. California: Elsevier Science

Green, D. W. & Willhite, G. P. (1998). Enhanced Oil Recovery, Society of Petroleum Engineers.

Huebner, K. H. (2001) The Finite Element Method for Engineers, 4th ed. New York: Wiley

Institute of Petroleum Engineering Heriot-Watt (2010), Heriot-Watt University - Reservoir Simulation. Edinburgh: Heriot-Watt University

Liu, G. R. (2003) Finite Element Method a Practical Course. Oxford: Butterworth-Heinemann

Maghsood, A.D., & Brigham, W.E. (1982) *Analysis of unit Mobility Ratio Well to Well tracer flow to determine reservoir heterogeneity.* California: Stanford University Petroleum Research Institute

Nunge, R. J. & Gill, W. N. (1969) *Mechanisms Affecting Dispersion and Miscible Displacement.* Flow through porous media symposium Vol 61 No 9

Schlumberger 2012. Eclipse Technical Description* reservoir simulation software. Version 2010.2 ed.

Schlumberger (2006). Reservoir Simulation Application Training Course and (Eclipse) Workshop. Denver and Houston: Schlumberger

Wong, P. Z. (1996) Methods of the Physics of Porous Media. San Diego: Elsevier Science

Xuan Zhang, S 2011, Upscaling of the Two-Phase Flows in Petroleum Reservoirs. Ph.D. Thesis, Technical University of Denmark

Zemel, B. (1995) tracers in the oil field. Amsterdam: Elsevier Science